10-5-2017

A model for soot load estimation in a Gasoline Particulate Filter using a Radio Frequency sensor

Angela Fiano
University of Windsor

A model for soot load estimation in a Gasoline Particulate Filter using a Radio Frequency sensor

By

Angela Fiano

A Thesis
Submitted to the Faculty of Graduate Studies
through the Department of **Mechanical, Automotive and Materials Engineering**
in Partial Fulfillment of the Requirements for
the Degree of **Master of Applied Science**
at the University of Windsor

Windsor, Ontario, Canada

2016

A model for soot load estimation in a Gasoline Particulate Filter using a Radio Frequency sensor

by

Angela Fiano

APPROVED BY:

_____

X. (Iris) Xu

Civil and Environmental Engineering

_____

C. Novak

Mechanical, Automotive and Materials Engineering

_____

A.Sobiesiak, Advisor

Mechanical, Automotive and Materials Engineering

09/13/2017

DECLARATION OF ORIGINALITY

I hereby certify that I am the sole author of this thesis and that no part of this thesis has been published or submitted for publication.

I certify that, to the best of my knowledge, my thesis does not infringe upon anyone's copyright nor violate any proprietary rights and that any ideas, techniques, quotations, or any other material from the work of other people included in my thesis, published or otherwise, are fully acknowledged in accordance with the standard referencing practices. Furthermore, to the extent that I have included copyrighted material that surpasses the bounds of fair dealing within the meaning of the Canada Copyright Act, I certify that I have obtained a written permission from the copyright owner(s) to include such material(s) in my thesis and have included copies of such copyright clearances to my appendix.

I declare that this is a true copy of my thesis, including any final revisions, as approved by my thesis committee and the Graduate Studies office, and that this thesis has not been submitted for a higher degree to any other University or Institution.

ABSTRACT

Gasoline Direct Injection (GDI) engines represent a promising technology for facing the more and more stringent limits imposed by emission regulations. However, one of the drawbacks of GDI engines compared to PFI engines is the production of soot. One of the possible solutions to reduce the amount of soot emitted in the atmosphere, among the different existent strategies, is the Gasoline Particulate Filter (GPF). Nowadays, the most common device in cars for monitoring the filter state and trigger the regeneration event is the differential pressure sensor. However, this provides an indirect measure of the soot state of the filter using a predictive model implemented in the Electronic Control Unit (ECU). A valid alternative, in laboratory environment, is represented by the Radio Frequency sensor. The objective of the study is to determine if a correlation exists between the output of the RF sensor and the amount of soot in the filter. The final outcome will be an analytical model that uses the average forward gain recorded from the Radio Frequency sensor and the exhaust gas temperature that can be used to estimate the amount of soot on the filter during both loading and regeneration phases. Moreover, with the output of the model during the regeneration event, it will be possible to understand when the soot oxidation starts and to distinguish the different soot reactivity, i.e. how it differently oxidizes during regeneration.

DEDICATION

A mia madre, mio padre,

mia sorella e mia nonna.

Con me, sempre.

ACKNOWLEDGEMENTS

This work represents the end of my academic life; in few months, I will not be a student anymore. I will work, have responsibilities, cooperate with many people and deal with any type of unforeseen circumstances. If I am able to face, without fear, my “new life” it is because of this experience. I have been working with a lot of different people, and I learnt so many things from them that I am more than excited to start my career.

First of all, I want to thank my CTC advisors, Jeff Wuttke and Jordan Easter; you supported me continuously and helped me every time I needed it. Jordan, thank you for your patience and for the time you dedicated to me. More than that, you and Jeff made me understand that it is fundamental to love your job.

I would like to express my deepest appreciation to my academic advisors at University of Windsor and Politecnico di Torino, Dr. Andrzej Sobiesiak and Prof. Federico Millo who assisted me and guided me during the development of this thesis.

Great thanks to my advisor at Centro Ricerche Fiat, Vittorio Doria before and Massimo Ferrara after. Thank you, Vittorio, for putting me in contact with this fantastic team at the CTC; this project has been great. I really appreciated your commitment in finding a project so innovative. Thank you, Massimo, for encouraging me and always giving me your support despite the distance.

Words are not enough to thank the coordinators of this project; Dr. Jennifer Johrendt, Prof. Giovanni Belingardi, Edoardo Rabino and Mohammed Malik. You gave us the opportunity to take part in this experience, which changed us forever.

Finally, I thank my Family and my Friends from the bottom of my heart. Your support makes me feel strong, I could reach my goals because you were and are always on my side. Eleonora, Giuseppe, Ilaria, Livia, Michele, Morgana, non avrei potuto affrontare quest’anno senza di voi. Grazie per I vostri sorrisi e le vostre parole, mi siete mancati ogni giorno di quest’anno. Abby, Alan, Alessio, Cassie, Chris, Donia, Justus, Marie, Mike, Regina, Renata, Siddique, I am so grateful I could spend this year with you! I wish I could

have you going in and out of our house for all my life. You gave me more reasons to love this experience; thank you for sharing this time with me. Mike, thank you for introducing us to the Canadian life and it wouldn't have been the same without you.

Mamma, papa', Giorgia, grazie per esserci stati incondizionatamente e costantemente, grazie perche' posso contare sempre su di voi; questa tesi e' dedicata a voi. Grazie ai miei cugini, ai miei zii, a mia nonna, alla mia splendida famiglia; sempre al mio fianco, sempre dalla mia parte.

Agostino, Benedetto, Federico, Simone and Wenzhou, I shared this whole year with you, all days, all pains, all joys, all travels, everything, I enjoyed every second I spent with you and I don't regret anything. You can rely on your Angelique, Angelocca, Angelflock, Angelfiocco, Angelsport, Angelina, Angel-whatever for the rest of your life.

I couldn't have imagined to live so close to some people who are not my family. I couldn't have imagined to love you as much as I do. (I will always think of you when I make cakes).

TABLE OF CONTENTS

DECLARATION OF ORIGINALITY iii

ABSTRACT iv

DEDICATION v

ACKNOWLEDGEMENTS vi

LIST OF TABLES x

LIST OF FIGURES xi

LIST OF APPENDICES xiv

LIST OF ABBREVIATIONS xv

1. INTRODUCTION 1

1.1 Background 1

1.2 Statement of the purpose 2

2. LITERATURE REVIEW 3

2.1 Gasoline Direct Injection 3

2.1.2 GDI Particulate emission 7

2.1.3 Gasoline Soot Oxidation 10

2.2 Gasoline Particulate Filter 11

2.3 Differential pressure sensor 16

2.4 Radio Frequency sensor 18

3. METHODOLOGY 27

3.1 Laboratory setup 27

3.2 Test procedure 34

3.2.1 Clean Regeneration 35

3.2.2 Test conditions (Loading) 36

3.2.3 Filter Regeneration 39

3.2.4 Final Test 40

4.1 Raw data discussion 41

4.2 Standard Test - Clean Regeneration 44
4.3 Standard Test - Loading 46
4.3.1 Early SOI 46
4.3.2 Late SOI 47
4.4 Filter Regeneration 49
4.5 Final test 54
4.6 Repeatability of experiments 56
5. MODEL AND RESULTS 58
5.1 Theory 59
5.2 Model – Loading 60
5.3 Model – Regeneration 62
5.4 Results – Loading 63
5.5 Results – Regeneration 67
6. CONCLUSIONS AND FUTURE WORK 71
6.1 Conclusions 71
6.2 Future work 72
APPENDIX 74
Appendix A 74
Appendix B 76
REFERENCES 80
VITA AUCTORIS 84

LIST OF TABLES

Table 1: EU Emission Standards for Passenger Cars. e. applicable only to vehicles using DI engines; f. 0.0045 g/km using the PMP measurement procedure; g. 6.0x10^12 1/km within first three years from Euro 6 effective dates. 1
Table 2: CARB LEV III particulate matter emission standard for passenger cars [6]. 2
Table 3: Testing engine specifications. 29
Table 4: Coated and uncoated GPF characteristics. 30
Table 5: Data elements available via serial communication interface [31]. 33
Table 6:Clean regeneration engine operating conditions. 36
Table 7: Engine operating parameters for the three different loading conditions. 38
Table 8: Loading operating conditions with relative duration. 39
Table 9: Engine operating conditions during filter regeneration phases. 40
Table 10: Final test engine operating conditions. 40
Table 11: Clean filter, Soot loaded filter weights and amount of soot accumulated during the loading phases. 49
Table 12: Soot quantities accumulated in the early SOI, late SOI and low injection pressure loading cases. 53
Table 13: Values of the soot weights, amount of soot predicted by the model and error. 65
Table 14: Uncoated GPF weight values with relative temperature recorded during the final test. 75
Table 15: Final test weights for the uncoated GPF normalized with respect to temperature. 76
Table 16: Dataset used for the creation of the model for the loading phase. 77
Table 17: Dataset used for the creation of the model for the regeneration phase. 78

LIST OF FIGURES

Figure 1: Comparison of the PFI and GDI mixture preparation systems [2]. 3
Figure 2: Homogeneous and stratified charge mode [1]. 4
Figure 3: GDI engine operating modes depending on load and speed [2]. 4
Figure 4: Typical engine exhaust size distribution both mass and number weightings are shown [13]. 7
Figure 5: Process leading to net production of particulates [14]. 9
Figure 6: Skeletonized pictures of GDI soot, heavy-duty diesel soot and carbon black [15]. 10
Figure 7: 90% oxidation timing as a function of ash fraction present in the soot at low and high soot for different engine operating conditions [16] 11
Figure 8: Wall flow substrate: inlet cell pattern (above), flow pattern (below) [24]. 12
Figure 9: Two different filtration mechanisms: Depth filtration (left) and Cake filtration (right) [24]. 13
Figure 10: Average particle number size distribution over the FTP-75 drive cycles for the different vehicles fuels and configurations [21]. 14
Figure 11: PN evolution over mileage for NEDC, WLTC and Artemis cycles with GPF [25]. 15
Figure 12: schematic representation of the DPS [18]. 17
Figure 13: Bosch "DS-D2" differential pressure sensor [28] 17
Figure 14: GE Accusolve RF sensor with two antennas [31]. 19
Figure 15: Schematic of a radio frequency (RF) soot sensor installed on a filter [23]. 19
Figure 16: Effect of soot and ash accumulation in a DPF on the RF sensor signal [33]. 21
Figure 17: Electric field distribution for the first resonant mode [34]. 21
Figure 18: RF sensor response compared to pressure drop over steady-state loading and regeneration cycles [33]. 22
Figure 19:Comparison of RF sensor with total engine-out PM emission over transient test cycles [33]. 23
Figure 20: Direct comparison between RF sensor output and TEOM cumulative PM mass data [33]. 23
Figure 21:Comparison of normalized pressure drop signal and PM cumulative soot mass [33]. 24
Figure 22: RF response during high DPF soot load active regeneration event [35]. 24
Figure 23: Influence of gas temperature variation on the averaged transmission parameter of the soot-free DPF, 3.39 g/l_{DPF} loaded DPF and 5.29 g/l_{DPF} loaded DPF [36]. 25
Figure 24: Schematic configuration of engine, GPF, thermocouples, differential pressure sensor and RF sensor setup. 27
Figure 25: Engine used in the laboratory for experiments. 28
Figure 26: Uncoated (left) and coated (right) filters. 29

Figure 27: Thermocouples applied on the GPF. 30
Figure 28: Scale used to weigh the filter. 31
Figure 29: Amphenol RF soot sensor [31]. 31
Figure 30: RF sensor antennas. 32
Figure 31: Plot of the first vector of Forward Gain vs. frequency, in a GPF loading case.. 34
Figure 32: Mass of soot oxidized vs. time for different engine operating conditions. 37
Figure 33: Black carbon soot concentration of soot produced in the four different operating conditions. 38
Figure 34: Average forward gain as a function of time, captured for early SOI conditions, in the case of the coated filter. 42
Figure 35: Average forward gain as a function of time, captured for early SOI conditions, in the case of the uncoated filter. 42
Figure 36:Forward Gain vs. Frequency at different time instant during early SOI loading test of uncoated filter. 43
Figure 37: Trend of T_e at inlet and outlet of the GPF and Radio Frequency sensor output vs. time during clean regeneration for the uncoated filter. 44
Figure 38: Trend of T_e at inlet and outlet of the GPF and Radio Frequency sensor output vs. time during clean regeneration for the coated filter. 45
Figure 39:Trend of T_e at inlet and outlet of the GPF and Radio Frequency sensor output vs. time early SOI loading for the uncoated filter. 46
Figure 40: Trend of T_e at inlet and outlet of the GPF and Radio Frequency sensor output vs. time early SOI loading for the coated filter. 47
Figure 41: Trend of T_e at inlet and outlet of the GPF and Radio Frequency sensor output vs. time late SOI loading for the uncoated filter. 48
Figure 42: Trend of T_e at inlet and outlet of the GPF and Radio Frequency sensor output vs. time late SOI loading for the coated filter. 48
Figure 43: Trend of T_e at inlet and outlet of the GPF and Radio Frequency sensor output vs. time of early SOI soot produced regeneration for the uncoated filter. 50
Figure 44: Trend of T_e at inlet and outlet of the GPF and Radio Frequency sensor output vs. time of early SOI soot produced regeneration for the coated filter. 50
Figure 45: Trend of T_e at inlet and outlet of the GPF and Radio Frequency sensor output vs. time of early SOI soot produced regeneration with DFSO event for the uncoated filter. 52
Figure 46: Comparison between regeneration phases of early SOI, late SOI and low injection pressure loading cases. 52
Figure 47: Differential pressure sensor output for early SOI (blue), late SOI (orange) and low injection pressure (red) test regeneration events. 53
Figure 48: Final test Radio Frequency output and inlet and outlet GPF T_e trends as function of time. 55
Figure 49: Trend of soot accumulation as function of time determined through the final test 55
Figure 50: Comparison between two early SOI tests RF output and inlet GPF T_e. 56

Figure 51: Soot amount as a function of average forward gain at constant temperature values. 61
Figure 52: Surface fitting of key points, using Matlab curve fitting tool. 61
Figure 53: Example of dataset retrieved from experiments. 62
Figure 54:Soot as a function of time for the early SOI test 1 condition testing as obtained from the surface fitting model. 64
Figure 55:Soot as a function of time for the late SOI tenting conditions as obtained from the surface fitting model. 64
Figure 56:Soot as function of time for the early SOI test 2 conditions as obtained from the surface fitting model. 65
Figure 57:Soot as a function of average forward gain for late SOI and early SOI conditions. 66
Figure 58: Soot values as function of average forward gain in the two cases of early SOI tests. 66
Figure 59: Soot oxidation trend obtained from the model in the case of early SOI produced soot and T_e trend as function of time during regeneration phase. 68
Figure 60: Soot oxidation trend obtained from the model in the case of late SOI produced soot and T_e trend as function of time during regeneration phase. 68
Figure 61: Soot oxidation trend obtained from the model in the case of low injection pressure produced soot and T_e trend as function of time during regeneration phase. 69
Figure 62: Comparison between normalized soot oxidation at 566 ºC for the three different operating conditions. 69
Figure 63: Soot oxidation as a function of time during regeneration of early SOI produced soot before the start of DFSO. 70
Figure 64: Soot oxidation as a function of time during regeneration of early SOI produced soot after the end of DFSO 70
Figure 65: Schematic configuration of weighing apparatus. 74
Figure 66: GPF weights as a function of temperature, collected during the final test for the uncoated GPF. 75
Figure 67: Plot of the dataset created to normalize GPF temperature. 76

LIST OF APPENDICES

Appendix A…… 76

Appendix B…… 79

LIST OF ABBREVIATIONS

RF	Radio Frequency
ICE	Internal Combustion Engine
GDI	Gasoline Direct Injection
PM	Particulate Matter
CARB	California Air Resources Board
LEV	Low Emission Vehicle
EPA	Environmental Protection Agency
DPF	Diesel Particulate Filter
GPF	Gasoline Particulate Filter
EU	European Union
PMP	Particle Measurement Program
PN	Particle Number
PFI	Port Fuel Injection
ECU	Electronic Control Unit
EOI	End Of Injection
SOI	Start of Injection
EGR	Exhaust Gas Recirculation
TWC	Three Way Catalyst
HC	HydroCarbons
NEDC	New European Driving Cycle

TGA	Thermo Gravimetric Analysis
FTP	Federal Test Procedure
WLTC	Worldwide harmonized Light Vehicles Test Cycle
E0	Ethanol free gasoline
E10	Gasoline mixture with 10% ethanol
DPS	Differential Pressure Sensor
TEOM	Tapered Element Oscillating Microbalance
DFSO	Deceleration Fuel Shut Off
BTDC	Before Top Dead Center
BMEP	Brake Mean Effective Pressure
Cpsi	Cells per square inches
Pt	Platinum
Pd	Palladium
Rh	Rhodium

1. INTRODUCTION

1.1 Background

Motivated by more and more stringent limits in the emission standard regulations and fuel economy targets, carmakers are working on the development of new technologies to improve efficiency of Internal Combustion Engines (ICE). One promising solution is Gasoline Direct Injection (GDI) technology [1] [2] [3], which is gaining market due to its superior fuel control and improvement in charge cooling as compared to common Port Fuel Injection engines [3]. In fact, due to the direct injection configuration, there is the potentiality of operating without throttling (successful approach used in Diesel engines), reducing pumping work and increasing expansion stroke work, with a possible improvement in the fuel economy [2]. On the other hand, there is the necessity of a sophisticated and optimally designed fuel injection hardware, which allows the correct preparation of the mixture cloud over the entire operating range of the engine [2].

Despite all these positive aspects, it was found that the amount of Particulate Matter (PM) produced by this kind of engine may not be compliant with the incoming regulations [3]. In fact, particulate emissions are now regulated also for gasoline engines with the new Euro 6 regulation for the European countries, California Air Resources Board (CARB) Low Emission Vehicle (LEV)III regulation for California and Environmental Protection Agency (EPA) Tier 3 for the United States [4].

Since the Diesel Particulate Filter (DPF) is an established emission control method for Diesel engines for several years, the usage of the same technology in Gasoline engines seems an obvious option to reduce PM emissions [5].

In this work, reference will be done to the European Union (EU) and to Californian emission standards, which is known as one of the most stringent emission regulations [6]. In Table 1, EU emission standards are summarized:

Table 1: EU Emission Standards for Passenger Cars. e. applicable only to vehicles using DI engines; f. 0.0045 g/km using the PMP measurement procedure; g. 6.0x10^12 1/km within first three years from Euro 6 effective dates.

Stage	PM $\left[\frac{g}{km}\right]$	PN $\left[\frac{\#}{km}\right]$
Euro 6 (Gasoline)	$0.005^{e,f}$	$6.0x10_{e,g}^{11}$

Particle emissions have always been regulated for Diesel engines, but the limits have been defined only for the Particle Matter mass (PM). Starting from Euro 5b, a Particle Number (PN) limit has been set. Moreover, with the increasing market share of GDI vehicles, gasoline particle emissions have been legislated. In fact, with Euro 6 starting from September 2014, both PN and PM limits of 6 x 10^{12} (initially, to be set at 6 x 10^{11} after three years from the Euro 6c effective dates), and 5 mg/km must be respected [7].

As it is possible to see in the Table 2, the particle matter mass limit will be lowered to 1 mg/mi by 2025, both for Petrol and Diesel engines, implying that all direct injection vehicles may be equipped with particulate filters [6].

Table 2: CARB LEV III particulate matter emission standard for passenger cars [6].

Stage	PM limit [$\frac{mg}{mi}$]	Phase-in
LEV III	3	2017-2021
	1	2025-2028

1.2 Statement of the purpose

The purpose of the current study is to evaluate the application of a Radio Frequency sensor as an instrument in laboratory tests to check the soot loading state after correct calibration. The sensor will be applied to GPFs to monitor its state during both loading and regeneration phases and to capture the differences in the soot reactivity during regeneration events. To do this, a model will be developed for simulating soot accumulation and soot oxidation rate using data collected from tests.

Nowadays, one the most common device used to check the soot state of the filter and consequently to trigger any regeneration events is the differential pressure sensor [8]; Radio Frequency sensor represents a complementary device with the potentiality of giving more accurate information on the amount of soot loaded on the filter and monitor the regeneration event, checking soot oxidation rate, detecting the different soot reactivity and eventually evaluating the right regeneration duration.

2. LITERATURE REVIEW

2.1 Gasoline Direct Injection

As abovementioned, GDI engines represent a promising alternative to Port Fuel Injection (PFI) engines; most of its advantages are attributable to the high flexibility of the modern electronic fuel injection system [2]. Firstly, it is important to underline the differences between PFI and GDI. The most evident one is the mixture preparation strategy which is illustrated schematically in the Figure 3:

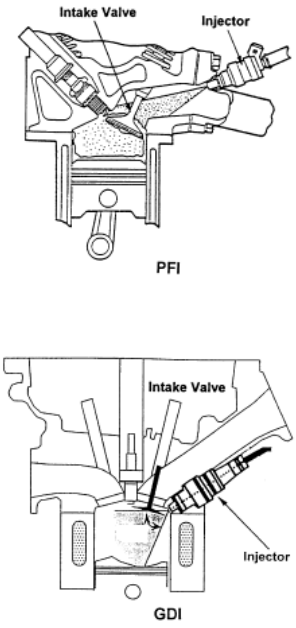

Figure 1: Comparison of the PFI and GDI mixture preparation systems [2].

In the PFI engine the injector is positioned in the intake manifold and the fuel is injected into the intake port of each cylinder. In this case the mixture has time to become homogeneous; on the other hand, during cranking and cold starting part of the liquid fuel remains in the intake valve area of the port due to low temperature conditions in the combustion chamber. A metering error derives from this phenomenon, due to partial vaporization of the fuel, and more fuel than the ideal stoichiometric required, needs to be supplied [2]. Alternatively, in GDI engines, the fuel is injected directly into the cylinders at high pressure, avoiding the problems related to the wall wetting in the port, allowing a better control of the metered fuel for each combustion event. Moreover, the higher injection pressure (4 – 13 MPa vs. 0.25 – 0.45 MPa for PFI) helps the atomization and vaporization of the fuel [2].

GDI engines essentially operate in two different charge modes: stratified and homogeneous charge.

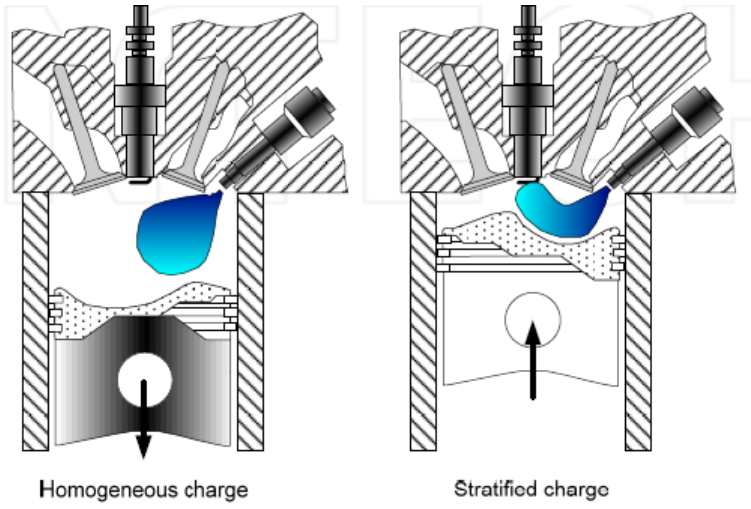

Figure 2: Homogeneous and stratified charge mode [1].

The stratified charge is obtained with late injection, so the fuel is injected during the compression stroke. Instead the homogeneous mixture is created when the fuel is injected during the intake stroke, with an early injection [2].

The Electronic Control Unit (ECU) selects one of these two charge modes continually changing the air fuel ratio [2]. The stoichiometric air fuel ratios for petrol engine is 14,7:1 by weight, but in lean mode it is possible to have air fuel ratio as high as 65:1.

In Figure 3, the different possible operating modes are illustrated.

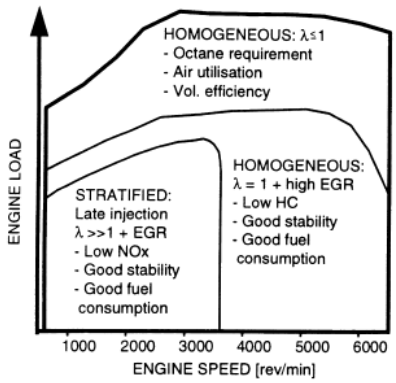

Figure 3: GDI engine operating modes depending on load and speed [2].

At low engine speeds and loads the stratified charge mode is used. In this case the late injection is commanded, meaning that fuel is injected shortly before the ignition, so a very rich mixture is created in the zone of the spark plug (stratification) but the overall charge is very lean, reducing significantly fuel consumption [9]. This reduction is due to unthrottled operation which reduces pumping losses and heat losses [2]. On the other hand, the very lean mixture causes the increase in the production of NOx, and for this reason the exhaust gas recirculation (EGR) is activated in this mode. Moreover, soot can form due to the charge being very rich nearby the spark plug [1]. During stratified operation, an important parameter to be controlled is the timing of the end of injection (EOI), since it determines the last liquid fuel which enters the combustion chamber. It has been reported that retarding the EOI timing causes a more rapid start of combustion, whereas an earlier EOI tends to shorten the combustion duration. When EOI is retarded the indicated specific fuel consumption have been demonstrated to be reduced, but unburnt hydrocarbons emissions are increased due to degraded mixture quality and a longer combustion duration [10].

For acceleration, full load and high engine speed, a stoichiometric or slightly rich air fuel ratio is set by the ECU, with the injection happening during the intake stroke. The charge becomes homogeneous, because there is a longer time for the mixture preparation. This strategy has been demonstrated to be comparable to that of conventional PFI engines [2].

Finally, a homogeneous charge mode has been reported to present some benefits also in case of cold starts and transients, because GDI engines have high performance due to increased volumetric efficiency and low tailpipe emissions, because of the possibility to use the three-way catalyst (TWC) [2].

It is now worthwhile to summarize the most important advantages and disadvantages of GDI engines. According to Zhao et al. [2], the theoretical main advantages are:

- Better fuel economy due to:
    - Reduced pumping loss (unthrottling in stratified charge),
    - Possible higher compression ratio (with injection during induction the charge is cooled, because there is not possibility of knock),
    - Reduced heat losses (during unthrottled operation),

    - Lower octane number required (with injection during induction the charge is cooled, because there is not possibility of knock),
    - Higher volumetric efficiency (with injection during induction the charge is cooled, because there is no possibility of knock).
- More precise air fuel control causing:
    - Less over-fueling during cold start (because of the absence of fuel film on the walls of the intake manifold),
    - More rapid starting and combustion stabilization especially if ambient temperature is lower (due to the absence of fuel film on the walls of the intake manifold. Moreover, direct injection allows better fuel atomization and consequent vaporization).
- Reduced CO_2 and HC emissions (due to improved combustion especially in cold-start conditions).

On the other hand, the major disadvantages are listed here:

- Complex injection technology requirements;
- Relatively high high-load NO_x emissions (during stratified charge operation);
- Higher particulate emissions;
- Difficulty in the control of the stratified charge combustion over the operating range;
- Higher electrical power and voltage requirements of the injectors and drivers;
- Increased wear for components of the fuel system due to higher pressure and low fuel lubricity.

Indeed, even if direct injection has been demonstrated to be very efficient for all the reasons abovementioned, differently from diesel engine, in gasoline engine there is the necessity of an ignition source. The location of the spark plug is fixed, then it is possible to operate in the unthrottled mode only for full load requirements. Mixture formation process is then a critical requirement, since it must be controlled both temporally and spatially to permit a stable combustion. Consequently, fuel injection system needs to be optimally designed to control the in-cylinder flow field [2].

2.1.2 GDI Particulate emission

As mentioned before, one of the biggest drawbacks of GDI engines is the emission of particles. Researchers have found that GDI engines generate a non-negligible amount of soot, both in mass and number, during cold start and transient operation due to the lack of time necessary to complete the combustion and to correctly create the mixture in the combustion chamber [11]. Both PM mass and PN produced by GDI have been demonstrated to be greater than those from a PFI vehicle, of 1 to 8 order of magnitude for the former [6], and by a factor of approximately 20 over the New European Driving Cycle (NEDC) for the latter [12].

"Particulate matter (PM) is defined as all substances, other than unbound water, which are present in the solid (ash, carbon) or liquid phases." [2]. It is common to refer to engine particulates as soot, which consists of solid carbon particles produced by combustion and on the surface of which some organic compounds have been absorbed (unburned hydrocarbons and oxygenated hydrocarbons) [2]. The size distribution of engine particulates has been found to have a trimodal distribution, with dimensions from several nanometers to several microns [13]. The three modes are known in the literature as:

- Nuclei mode (particle equivalent diameters < 50 nm)
- Accumulation mode (particle equivalent diameters from 50 to 1000 nm)
- Coarse mode (particle equivalent diameter > 1000 nm)

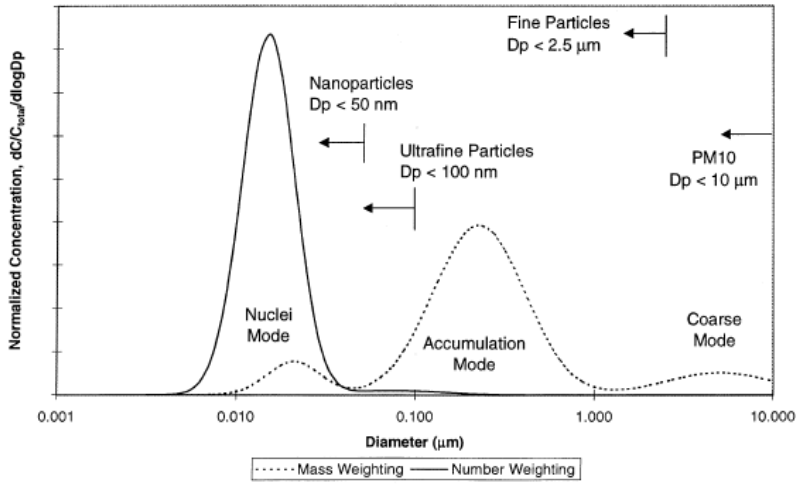

Figure 4: Typical engine exhaust size distribution both mass and number weightings are shown [13].

The nuclei mode particles are created during combustion and dilution. This mode dominates the number-weighted size distribution; on the other hand, it has a negligible impact on the number weighted size distribution. The accumulation mode, instead, derives from the agglomeration of nuclei mode particles, being consequently much heavier and less in number. In fact, they constitute the most significant contribution to the mass weighted size distribution. Finally, the coarse mode particles are not a direct product of the combustion, but derive from the solid residues present on the valves and chamber walls that sometimes can enter the exhaust manifold [13].

Soot particles form in fuel-rich flames or fuel rich parts of flames, and the formation process from a fraction of fuel takes few milliseconds. The major stages of the process are briefly presented:

- Particle formation. Due to oxidation and/or pyrolysis phenomenon of fuel molecules, the first condensed very small particles arise (nuclei), which usually include unsaturated hydrocarbons.
- Particle growth. This phase includes surface growth, coagulation and aggregation. During surface growth, most of the solid particles are generated since the gas-phase species are incorporated into the particulate phase. The amount of particles remains the same, but there is an increase in the amount of soot volume fraction. On the contrary during growth by coagulation, when particles collide and coalesce, the number of particles decrease and the soot volume fraction remain constant. At the end, it can also happen that particles aggregate into chains and clusters (adsorption and condensation) [14].

In Figure 5 the different processes are summarized. Even if they are represented as successive and discrete events, they could overlap and may occur concurrently in the combustion chamber [14]. The various phases presented before happen inside the cylinder, whereas the adsorption and condensation occur principally in the exhaust system. In the regulation of EPA for particulates, it has been specified that it is necessary to use an exhaust dilution tunnel to simulate the atmospheric dilution process.

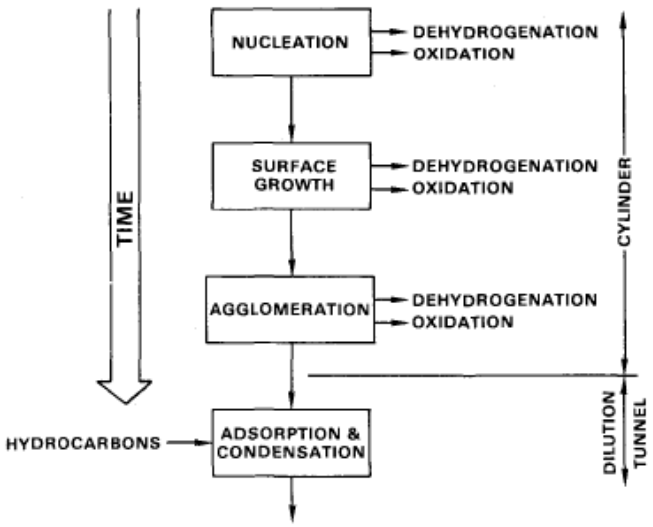

Figure 5: Process leading to net production of particulates [14].

To better understand soot formation in the GDI engines, nanostructures of primary particles have been investigated by Seong H. et al. [15]. Experiments were performed with a GDI engine operating at different conditions (rpm and torque), finding that GDI soot particles show less-ordered structures than carbon black and diesel soot. In fact, carbon black and diesel soot show similar features with long fringe layers, regularly paralleled, and not curved. On the other hand, soot samples presented fringe layers more curved and this characteristic suggest that GDI soot is less ordered than diesel soot, possibly due to the limited amount of hydrocarbons involved in the soot formation process, causing a delay in the graphitization of soot particles. Figure 6 shows GDI soot, diesel soot and carbon black skeletonized images, which present the characteristics abovementioned.

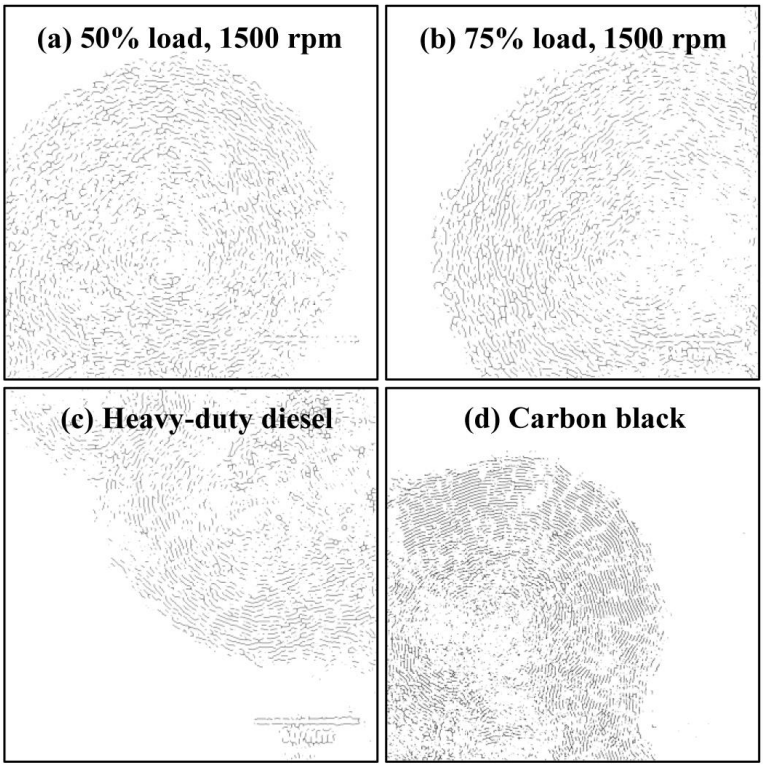

Figure 6: Skeletonized pictures of GDI soot, heavy-duty diesel soot and carbon black [15].

2.1.3 Gasoline Soot Oxidation

One of the objectives of this study is to determine if the Radio Frequency sensor can detect the differences in the reactivity of soot. During regeneration events, soot is oxidized i.e. chemical reactions happen which transform the solid particles to gaseous products (preferably CO_2). Much research has been conducted to explore the kinetics of diesel soot during regeneration in diesel particulate filter, whereas few studies can be found about oxidation characteristics and kinetics. Recent studies [16] have found that GDI soot is more reactive than diesel soot, but its oxidation characteristics remain unknown. It has been shown that reactivity varies due to variation that can occur during soot formation to fuel properties, local temperatures, local equivalence ratios, residuals from oil and fuel additives.

In previous works, different soot properties were found to be correlated with the changes in soot reactivity; among them it was determined that nanoparticle morphology plays a role in influencing soot reactivity [17] . If the soot presents an amorphous structure it is more likely that oxidation happens [18]. Increased unburnt hydrocarbons may influence soot reactivity too [19].

Ash has also been demonstrated to have an effect on soot oxidation. Seungmok et al. [20] analyze the oxidation characteristics of naturally aspirated homogeneous and stoichiometric GDI engine soot at different engine operating conditions and ash fraction, and compare the results with a model soot using thermo gravimetric analysis (TGA). They focused primarily on the effect of ash fraction on soot oxidation reactivity, analyzing soot samples with different percentage of ash. It was found that differently from diesel engines, ash has a major impact on soot oxidation, since its fraction is of an order of magnitude higher than in the diesel soot. Ash is composed principally of metallic elements, so it works as a catalyst for GDI soot, increasing its reactivity during oxidation.

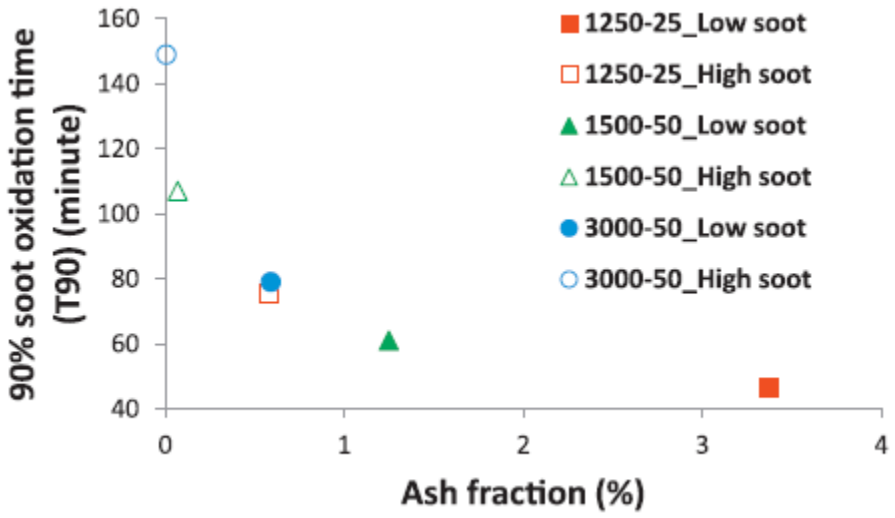

Figure 7: 90% oxidation timing as a function of ash fraction present in the soot at low and high soot for different engine operating conditions [16]

Typically, soot shows a three-stage oxidation with increased oxidation rates at the initial and final stages, and a relatively low rate at the intermediate stage [20].

2.2 Gasoline Particulate Filter

It happened during recent times that gasoline engines started to be considered in the definition of the PM emission standards. In fact, port fuel injection engines produce particulate emissions in the order of only 1% of those of diesel engines [2]. Due to increase in market share of gasoline direct injection engines, this limits cannot be restricted only to diesel engines; Euro 6 regulation and CARB LEV III imposed limits both for number and mass of PM emitted in the atmosphere by gasoline engines.

In order to address the challenge of GDI particulate reduction different methods can be adopted: adjusting the air/fuel ratio, the fuel injection strategy (timing, number of injections, injection pressure), the combustion phasing and the engine temperatures. However, even these calibration changes may not be enough to compensate with injector coking and variations in market fuels, therefore, as a post-emission control strategy, a gasoline particulate filter (GPF) may also be used to control and reduce the emission of soot [21]. It seems straightforward to try to apply the same technology to direct injection gasoline engines, even if filter parameter adjustments, (total volume, frontal area, substrate cell density, porosity, pore size, wall thickness and washcoat catalyst) are necessary due to the differences between diesel and gasoline engines exhaust emission [22].

Many different materials are used for filters (cordierite, silicon carbide, mullite, mullite/zirconia, exc. [23]), but the most common material for GPFs is cordierite.

Generally, the structure of the filter is known as a “wall flow” substrate, shown in Figure 8:

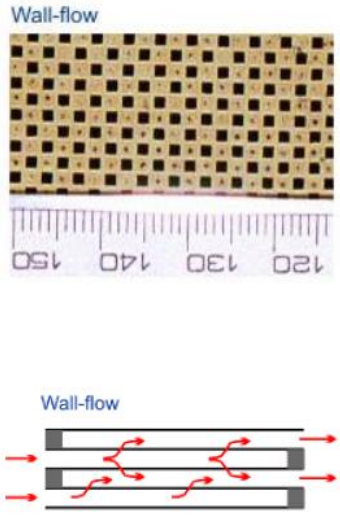

Figure 8: Wall flow substrate: inlet cell pattern (above), flow pattern (below) [24].

Channels are alternatively plugged at each end, to force the exhaust gas through the porous walls, where the particles are collected. When the filter is clean the soot particles are collected in the pores within the walls; then a soot layer is created on the surface of the channel which acts as a “filtration cake” increasing the filtration efficiency of the filter.

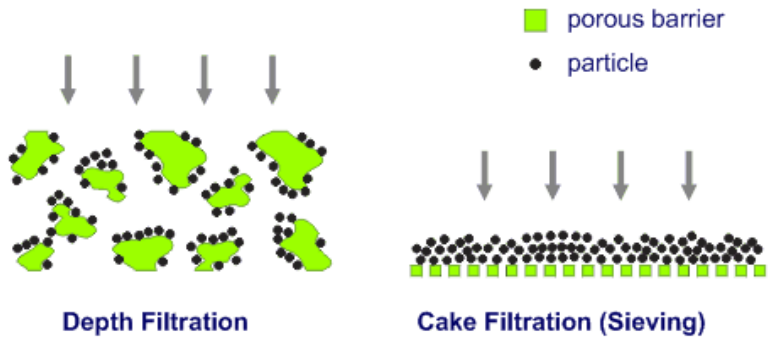

Figure 9: Two different filtration mechanisms: Depth filtration (left) and Cake filtration (right) [24].

Depth filtration is characterized by a lower pressure drop and lower filtration efficiency than cake filtration, due to the high porosity of the filter, which allows particles to go through filter walls. On the other hand, during cake filtration mode the efficiency is lower at the beginning, until the filtration cake reaches a sufficient thickness; then it increases because soot particles can hardly escape the "cake" layer. Moreover, the pressure drop increases with the cake layer thickening.

When the soot is trapped in the filter, the pressure drop (back pressure) starts to increase. After a certain time, the soot could obstruct the exhaust gas flow further increasing the backpressure. Then it is necessary to remove the accumulated soot by mean of the so-called regeneration process. It is also important to correctly set regeneration start: the level of soot cannot be too high otherwise the filter could be damaged by the process.

During regeneration, the soot is oxidized and according to the used regeneration strategy it is possible to classify the filters: there are active and passive G/DPFs. In the former case the temperature is increased to the point where the trapped soot starts oxidizing, whereas in the latter, engine parameters (like exhaust temperature and oxygen content) are controlled to determine the start of a regeneration event.

Chan et al. [21] compared the particle number size distribution for stock GDI, GDI post-GPF, and PFI configurations over the FTP-75 drive cycle using two different fuels E0 and E10. The results are shown in the following figure:

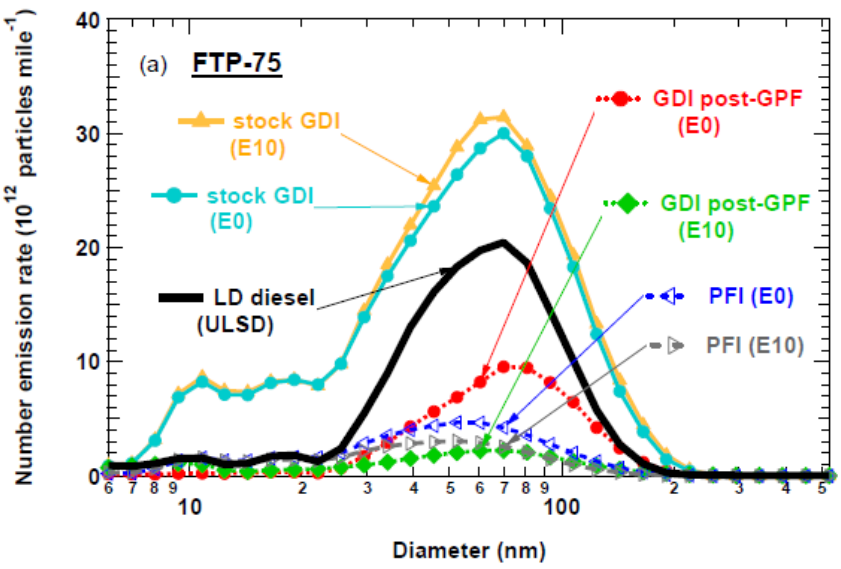

Figure 10: Average particle number size distribution over the FTP-75 drive cycles for the different vehicles fuels and configurations [21].

As it is possible to notice, both stock GDI engines are clearly out of emission limits. However, with the application of the filter tailpipe emissions are lower than that of a diesel engine with a DPF and even comparable to PFI particle emissions. The GPF could reduce the amount of soot with a filtration efficiency of 80-82% [21].

In a study by Waters et al. [25], the GPF filtration performance has been studied for the New European Driving Cycle (NEDC), Worldwide harmonized Light Vehicles Test Cycles (WLTC) and Artemis cycles in a durability test, to determine its behavior when it is aged. It has been demonstrated that, due to accumulated layer of ash resistant to regeneration events, the filtration efficiency increases over mileage [25].

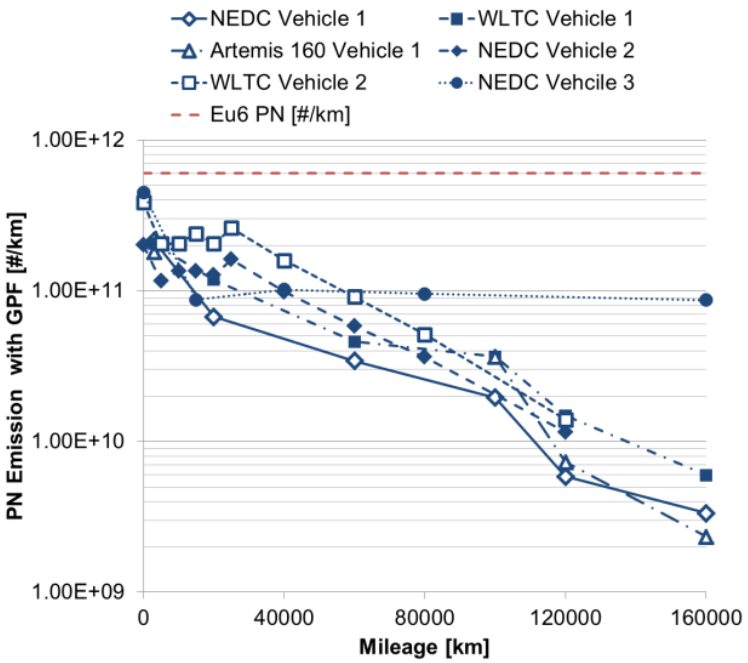

Figure 11: PN evolution over mileage for NEDC, WLTC and Artemis cycles with GPF [25].

In all cases filtration efficiency improved tending towards 99,9% [25].

Filtration efficiency is one of the parameters that can be different between GPFs and DPFs. According to Saito et. al [26] who studied the most influencing parameters on GPF performance, filtration efficiency in the case of a GPF could be reduced by lower soot emissions, which results in the creation of a thinner soot layer. This is different from DPFs, in which particle filtration is increased by the presence of soot layer in the cake filtration phase. On the other hand, a lower pressure drop across the GPF is generated if the soot layer is not thick, consequently lowering the fuel consumption [22]. It needs also to be considered that higher exhaust temperatures and flow rates of gasoline engines compared to diesel could increase the pressure drop, but also create the possibility of spontaneous regeneration events.

Another difference can be found in the amount of oxygen present in the exhaust of diesel and gasoline engines; in the latter, the mixture is principally stoichiometric and then almost all the oxygen is consumed in the combustion of the injected fuel. However, the TWC operation is optimized, but no oxygen is available in these cases if regeneration is needed. So it is only during deceleration and fuel cuts that oxygen excess is available for regeneration of the filter. A catalyst can be added to lower the regeneration temperature required for regeneration and to enhance

the oxidation process [22]. Anyway, the GPF is not a standard emission control device now, and research is being done for the characterization of GDI emissions to allow for proper design of GPFs and optimization of their operations. In particular, the regeneration event has to be taken under control, being a very critical and complex process.

Discussing about physical parameters, M. Görgen et al. [27] analyze the most important ones in their research:

- Total volume; it influences the backpressure and it is usually proportional to engine displacement. In the case of GPFs, the total volume can be either smaller than the engine displacement, with consequent better packaging options but limited soot storage capacity, or slightly bigger which are less cost effective but allow higher ash deposition and a long service lifetime.
- Frontal area; it is designed again for fitting the limited packaging space, and to minimize backpressure. In the former case a small frontal area is beneficial, whereas in the latter case it is preferable to have a high frontal area.
- Cell density; the most used substrate for coated GPF application are in 300 cpsi, which has been proved to be a good compromise between filtration efficiency and backpressure.
- Wall thickness: the configuration with 0.008 inches gives stability and at the same time high filtration.
- Three-way coating: its necessity depends on GPF application, catalyst design and engine raw emissions. If gaseous emissions need to be reduced precious metal coating is necessary, even if it increases backpressure significantly [3].

2.3 Differential pressure sensor

Accurate knowledge of the state of the particulate filter is fundamental to correctly trigger the regeneration event. Different sensors can be used in the after-treatment system to monitor the GPF actual conditions. In this laboratory research, two different sensors were mounted on the GPF and they will be shortly described:

- Differential pressure sensor (DPS or ΔP-Sensor);
- Radio Frequency sensor.

The DPS is the most common technology for the evaluation of the soot mass present on the DPF because they are simple, cheap and easy to be integrated in the exhaust system.

The ΔP-Sensor evaluates the pressure difference between upstream and downstream of the filter, i.e. the pressure drop. This value is transformed into an electrical signal and communicated to the ECU through a transmitter [23] as illustrated in Figure 12.

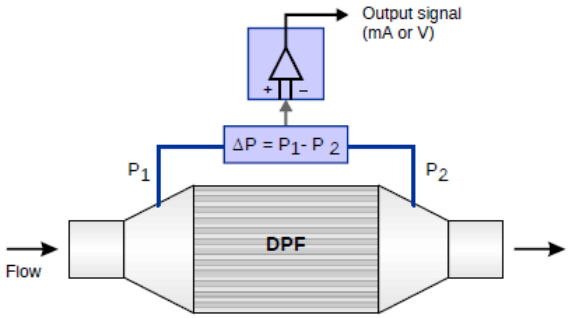

Figure 12: schematic representation of the DPS [18].

Numerous typologies of DPS are present on the market; most of them like the sensor Bosch DS-D2, like the one shown in Figure 13, are based on piezo-resistive working principle. A micromechanics membrane made of silicon with a Wheatstone bridge made of resistances is the element used to take measurements. The flange on the left is the connection on the car frame, the one on the right is connected to control unit. The two pipes on the bottom reach the exhaust gas flow before and after the DPF [28]. The resistors in this sensor are strain-gauge type, so that their properties change with deformation. When the sensor is exposed to different pressures, the membrane is deformed, and consequently the resistances in the bridge change.

Figure 13: Bosch "DS-D2" differential pressure sensor [28]

As before specified, two different filtration mechanisms take place in a particulate filter; so, when the particulate is accumulated, the pressure drop changes in different ways. At the beginning, the so-called “depth filtration” mode is characterized by a non-linear increase of the GPF pressure drop, because initially particles are accumulated in the porous walls of the filter, blocking the flow paths. Then, when the filtration mode changes to the so-called “cake filtration” mode, a soot layer starts to grow on the top of the wall, causing the pressure drop trend to have a linear trend with the accumulated soot.

Extensive work has been done to correlate the amount of soot accumulated in the filter with the relative pressure drop. The ECU estimates the soot mass in the filter based on the pressure drop that increases with the increasing amount of soot [28]. However, the pressure drop signal is not a direct measure of the soot mass present in the filter; indeed, the ECU exploits an empirical model to process the data acquired from DPS and other sensors. Based on this information it continuously estimates the actual soot load in the filter and compares it to a pre-programmed value, chosen to trigger regeneration. The regeneration trigger threshold must be carefully chosen because it determines the frequency of regeneration and has an impact on the fuel economy [29].

Due to this method limits, manufacturers usually adopt conservative approaches, considering a high safety factor to avoid excessive soot accumulation and uncontrolled filter regeneration. Consequently, the full soot storage capacity of the filter is not used, leading to unnecessary regeneration and more thermal stress on the filter. However, it is worth to consider that amounts of soot accumulated in GPFs are much lower than in DPFs, and this could not be enough to have a significant output from the differential pressure sensor. Then, there is the opportunity to optimize filter operation improving sensing and controls to accurately determine filter loading state [30].

2.4 Radio Frequency sensor

Radio frequency sensors represent an alternative technology that can be used to determine the current soot loading state of the GPFs, providing a direct measurement of the collected mass. This type of sensors is constituted by an electronic controller and one or two antennas. Antennas are designed to resist the same temperature range as the filter housing itself, and they are made of stainless steel coax terminating into a monopole antenna.

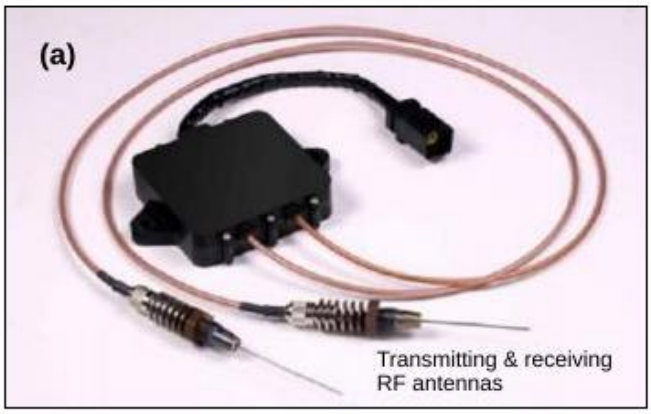

Figure 14: GE Accusolve RF sensor with two antennas [31].

In this soot measurement approach, one or more antennas are used to transmit and receive radio waves, in the range of the microwaves, through the soot-laden GPF, using the filter housing as a resonant cavity. The schematic configuration used in the tests is presented in Figure 15:

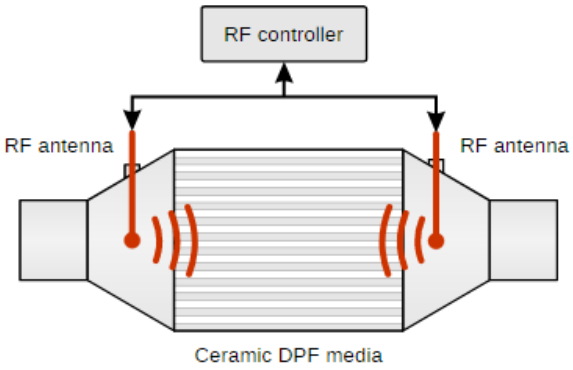

Figure 15: Schematic of a radio frequency (RF) soot sensor installed on a filter [23].

A signal is sent by the sensor control unit; the radio wave propagates through the filter and then is received by the antenna. The operating frequencies are chosen below the cut-off frequency of the exhaust pipe so that the signal is fully contained in the filter housing. As the signal passes, it changes its resonance characteristics because it is affected by the dielectric properties of the material (soot, ash) inside the filter. For this reason, Radio Frequency sensors can only be applied to non-conducting filter media, because conducting materials block the signal from penetrating the filter.

The dielectric properties above mentioned are:

- Permittivity of the material;
- Relative permittivity;
- Loss factor.

The permittivity of a material is defined as the measure of the material's ability to resist an electric field [32], and it is a complex number composed of two parts [33]:

Equation 1: Mathematical expression of material permittivity.

$$\boldsymbol{\varepsilon = \varepsilon' - i\varepsilon''}$$

The relative permittivity, instead, is a dimensionless quantity defined as the ratio of the absolute permittivity of the material and the electric constant (vacuum permittivity) [33]:

Equation 2: Mathematical expression of relative permittivity.

$$\varepsilon_R = \frac{\varepsilon'}{\varepsilon_0}$$

Finally, the loss factor is defined as:

Equation 3: Mathematical expression of loss factor.

$$tan\ \delta = \frac{\varepsilon''}{\varepsilon'}$$

And it influences the signal amplitude and the amount of transmitted power. For vacuum this value is equal to zero.

Soot shows a high degree of dielectric losses, and so it is eligible to be detected by Radio Frequency sensor. Therefore, this method exploits the differences in the dielectric properties of what is trapped into the filter (ash and soot) and the medium (air/exhaust). As soot and ash accumulate on the filter the RF sensor signal is directly affected [33]. In Figure 20, the result from Sappok et al. [33] is shown. When the frequency is changed, different resonant modes are established in the filter housing. The accumulation of soot and ash change the frequencies, amplitude and width of the resonant modes, but in two different ways. In fact, due to its high dielectric loss soot causes an attenuation of the resonant peaks, whereas ash, which has a

dielectric constant sufficiently different, causes the resonant frequency to shift. Hence, the RF signal characteristics may be directly correlated to both changes of soot and ash state in the filter [33].

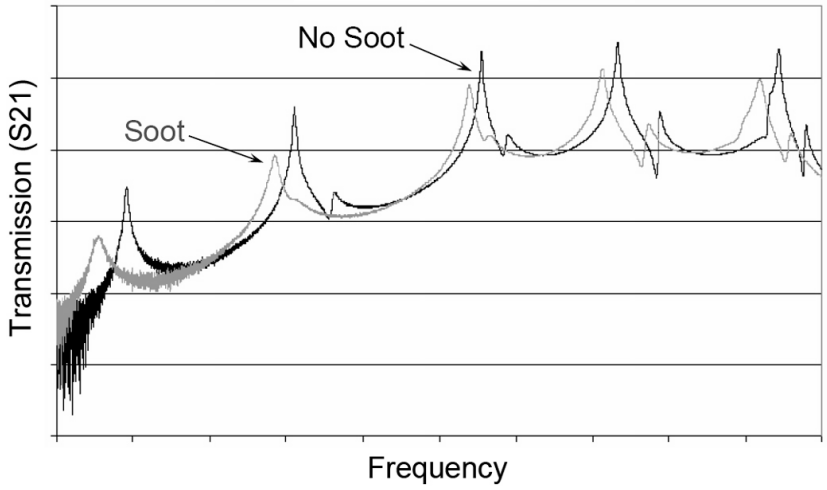

Figure 16: Effect of soot and ash accumulation in a DPF on the RF sensor signal [33].

Physically, the resonant peak modes represent the local areas where a high electric field is established at the various frequencies. Therefore, applying this method, it may be also possible to detect the spatial distribution of the accumulated material in the filter. Figure 17 by Sappok et al. [33] shows the electric field regions for the first resonant peak. Red and yellow colors indicate zone of high electric filed. This information of ash and soot distribution in the filter may be exploited for diagnostic application to detect anomalous soot and ash build-up [33].

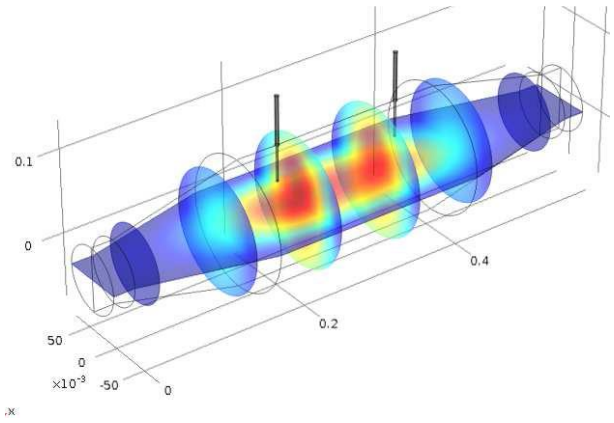

Figure 17: Electric field distribution for the first resonant mode [34].

Numerous studies can be found in the literature relating the Radio Frequency sensor response to the amount of soot present in a Diesel Particulate Filter during both steady-state and transient cycles. Moreover, temperature of the filter, exhaust gas flow and oxygen storage influence have been researched.

During steady-state engine operations for loading and regeneration phases, Sappok et al. [33] reported that RF signal demonstrated to be stable and not affected by exhaust flow variations, differently from pressure drop. Moreover, despite the high temperature reached during regeneration (>750 ºC) the Radio Frequency sensor output shows a stable linear response:

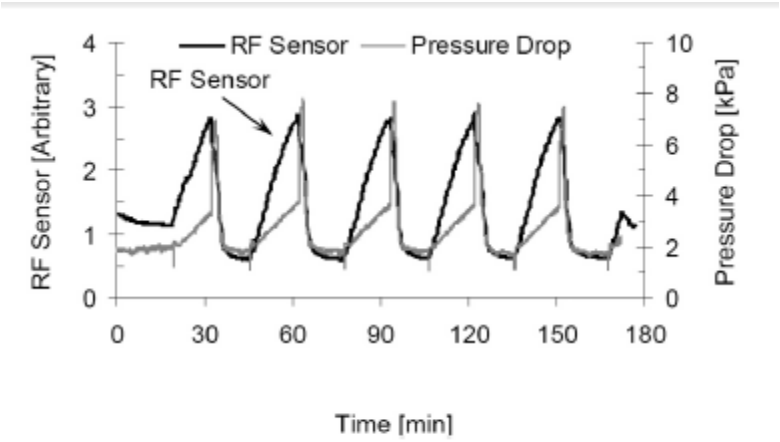

Figure 18: RF sensor response compared to pressure drop over steady-state loading and regeneration cycles [33].

In the same study by Sappok et al. [33] results from transient test cycles can be found. They show good agreement between the RF signal and the soot amount measured via tapered element oscillating microbalance (TEOM). The Radio Frequency sensor exhibits a fast response even during transient cycles, as well as a certain stability during the mild operation conditions of the test cycle. A direct comparison between the Radio Frequency response and the soot mass data is shown in Figure 19, where it is possible to notice that both Radio Frequency sensor and TEOM measure the cumulative amount of soot captured on the diesel particulate filter [33].

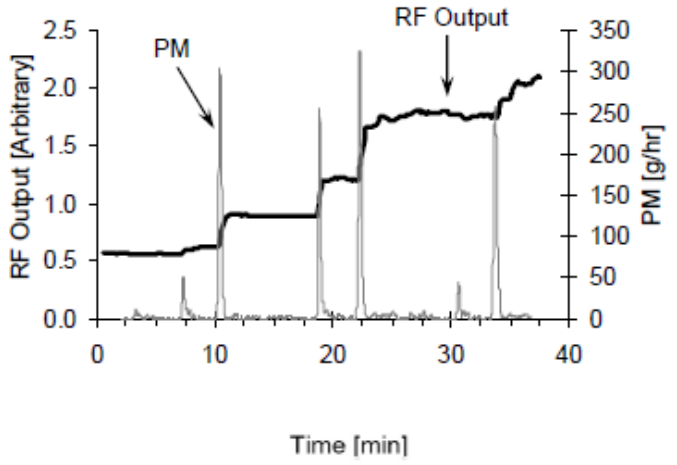

Figure 19:Comparison of RF sensor with total engine-out PM emission over transient test cycles [33].

Finally, a direct comparison between differential pressure sensor response and cumulative PM emissions is presented in Figure 20.

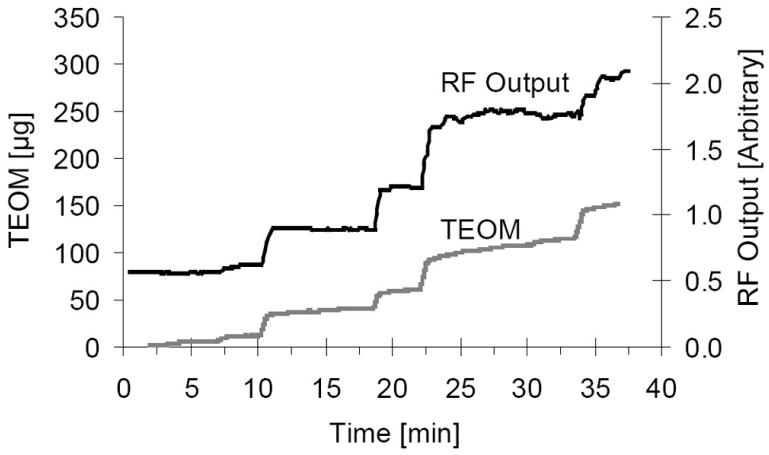

Figure 20: Direct comparison between RF sensor output and TEOM cumulative PM mass data [33].

Moreover, the trend shown in Figure 21 underlines that pressure drop appears to be more sensitive to transient variations in the exhaust temperature and exhaust flow conditions, even if the signal was normalized by the actual exhaust volumetric flow rate. Differently from Radio Frequency response, the differential pressure sensor output does not show all the transient peaks in the soot emissions [33].

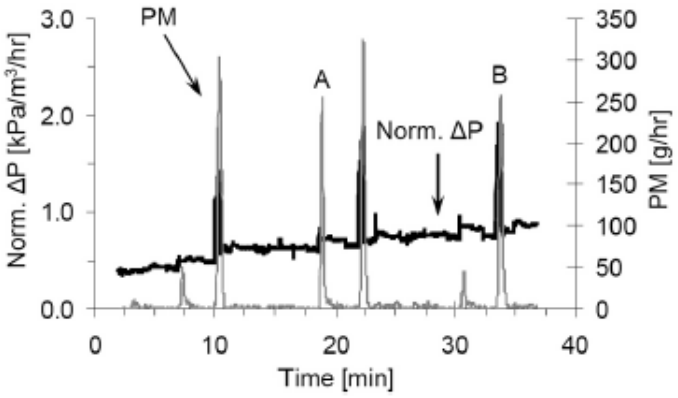

Figure 21:Comparison of normalized pressure drop signal and PM cumulative soot mass [33].

RF sensor response during regeneration events have been further studied by Sappok et al. [33] to demonstrate that regeneration could be optimized using this technology to monitor the particulate filter soot loading phases. In Figure 22, a typical Radio Frequency sensor response during an active regeneration event is presented:

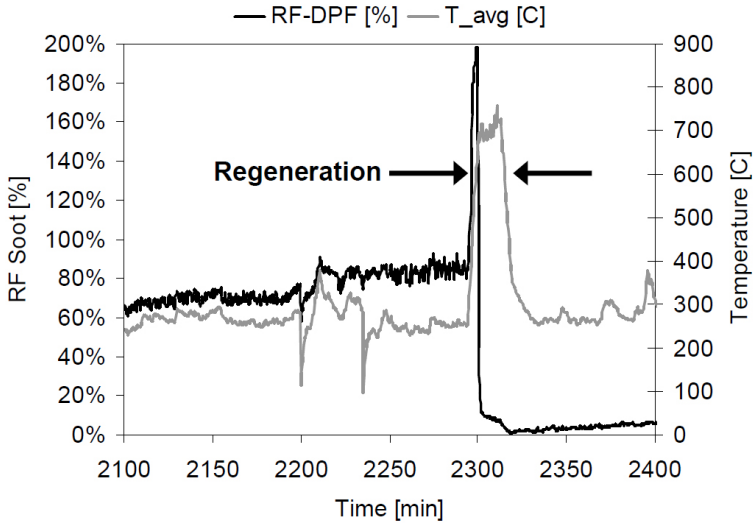

Figure 22: RF response during high DPF soot load active regeneration event [35].

The soot level in the particulate filter is relatively high; with increasing temperature, it is possible to notice a larger spike, demonstrating an increased sensitivity to higher temperatures. Soot oxidation is almost complete during the first half of the regeneration event, and the RF signal rapidly drops even if temperature remains at high level. The rapid decrease of the RF signal at elevated temperatures gives a high level of confidence that the soot has been completely oxidized before the regeneration event is stopped by the stock control system.

Consequently, by using RF sensor technology it could be possible to reduce active regeneration events time by around 50% based on these measurements [35].

In conclusion, gas variation effect on the RF sensor output at different soot levels is reported. Experiments have been performed to understand how the RF signal is affected by gas temperature to correct the correlation with soot amount loaded in the particulate filter. In the study by Feulner et al. [36] three filters loaded at 5.29 g/l$_{DPF}$ and 3.39 g/l$_{DPF}$ and soot-free, have been examined under temperature variation condition [36]. The outcome appears in Figure 27:

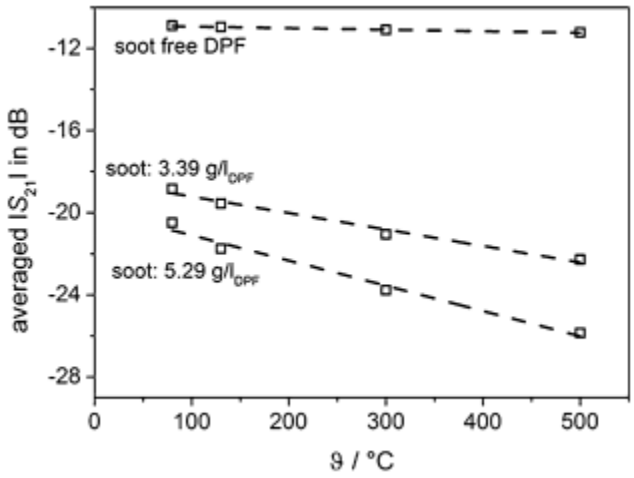

Figure 23: Influence of gas temperature variation on the averaged transmission parameter of the soot-free DPF, 3.39 g/l$_{DPF}$ loaded DPF and 5.29 g/l$_{DPF}$ loaded DPF [36].

The signal of the soot-free DPF results to be constant with respect to temperature variations, whereas in both medium and high soot loaded DPF the signal is linearly shifted towards lower values of the $|S_{21}|$ parameter. The slope of the curves changes with the differences in soot loaded, meaning that higher soot loaded DPFs are more affected by gas temperature variations. This phenomenon can be explained by the increased electrical conductivity of the soot present in the filter, which lead to a greater attenuation of the RF signal. Instead, as expected, in the soot-free filter, since no soot is present the $|S_{21}|$ parameter remains constant.

To conclude this chapter, a list of the most important outcomes of the studies found in the literature is presented:

1. Temperature affects the Radio Frequency performances due to the thermal dependent dielectric properties of the soot [36];

2. Radio Frequency sensor shows good repeatability over successive steady-state DPF loading and regeneration events, detecting even low-level engine PM emissions [33];
3. Based on Radio Frequency measurements regeneration intervals may be extended reducing filter thermal excursions minimizing temperature active regeneration events [33];
4. Regeneration duration may also be optimized during high temperature regeneration events, because Radio Frequency sensor has indicated rapid soot oxidation during the first half of regeneration event set by the stock controls [35].

Despite all the numerous studies carried out on the Radio Frequency sensor DPF application, very few or none information can be found on tests performed with gasoline particulate filters. Moreover, most of what is known is related to Radio Frequency sensor application during loading phases, so when the soot is accumulated. The aim of this work is to explore the use of Radio Frequency sensor for GPF use, with more focus on the regeneration event and soot oxidation process. Since previous analysis have demonstrated that the Radio Frequency sensor can provide a direct measurement of soot accumulation, the hypothesis is that after correct calibration it will be suitable for detecting the differences in the types of soot produced by GDI engine in different operating conditions.

3. METHODOLOGY

In this chapter the instrumentation and laboratory set-up used in Walter and Lay automotive engineering laboratory at University of Michigan, and the test procedure to perform each test will be described.

3.1 Laboratory setup

In Figure 24 the schematic configuration of the engine/GPF/RF sensor setup used for the experiments is shown:

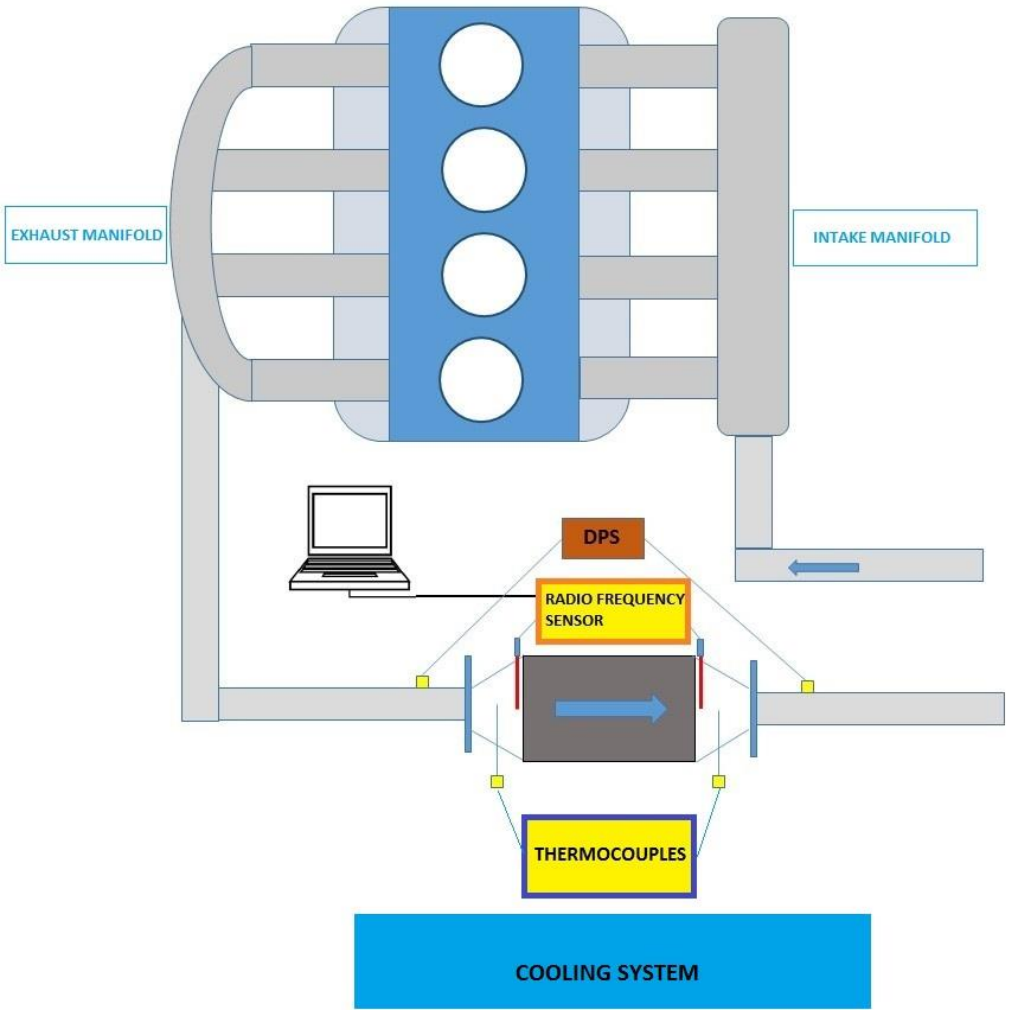

Figure 24: Schematic configuration of engine, GPF, thermocouples, differential pressure sensor and RF sensor setup.

The main components of the laboratory setup for this research are:

- Engine;
- Gasoline Particulate Filter;
- Thermocouples;
- Cooling system;
- Radio Frequency sensor;
- Differential pressure sensor.

These components will be described more in details in the next pages.

Moreover, a high precision scale was used to determine gravimetric measurements of the soot loaded; it will be also described further on.

The engine used for testing is a 2.0 liter, 4 cylinders turbocharged gasoline direct injection, and it is shown in Figure 25. The engine is run at medium to high load with a homogenous strategy. In Table 3 engine technical specifications are reported.

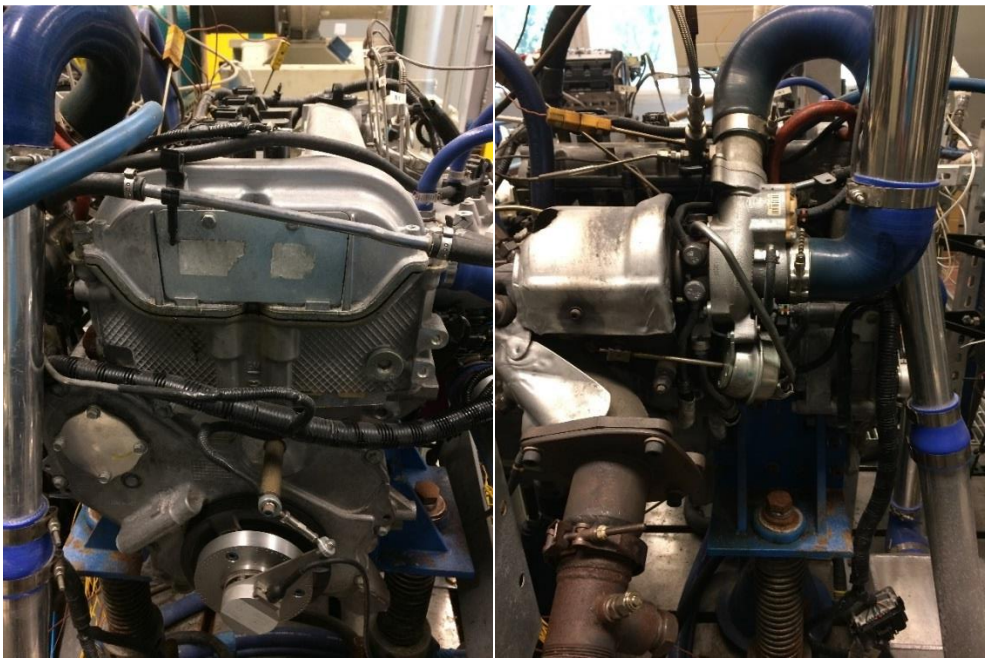

Figure 25: Engine used in the laboratory for experiments.

Table 3: Testing engine specifications.

Engine Specifications	
Bore	86 mm
Stroke	86 mm
Compression Ratio	9.2
Fuel Injection	side mounted wall guided
Turbocharger	K04
Valvetrain	dual VVT with 50°CA phasing

In the exhaust system of the engine a gasoline particulate filter is mounted. Two types of GPFs are used for these experiments: a coated and an uncoated filter shown in Figure 26:

Figure 26: Uncoated (left) and coated (right) filters.

The characteristics of the filters are summarized in Table 4:

Table 4: Coated and uncoated GPF characteristics.

Characteristics	Coated	Uncoated
Volume	1.4 L	1.4 L
Cell Geometry	300/8	300/8
Porosity	65%	65%
Material	Cordierite	Cordierite
Length	127 mm	127 mm
Diameter	118 mm	118 mm
Precious Metal Loading	yes	no

The two GFPs are the same, except for the presence of the catalyst in the case of the coated filter.

Exhaust gas temperature (T_e) is measured at the inlet and outlet of the monolith, using type K thermocouples shown in Figure 27.

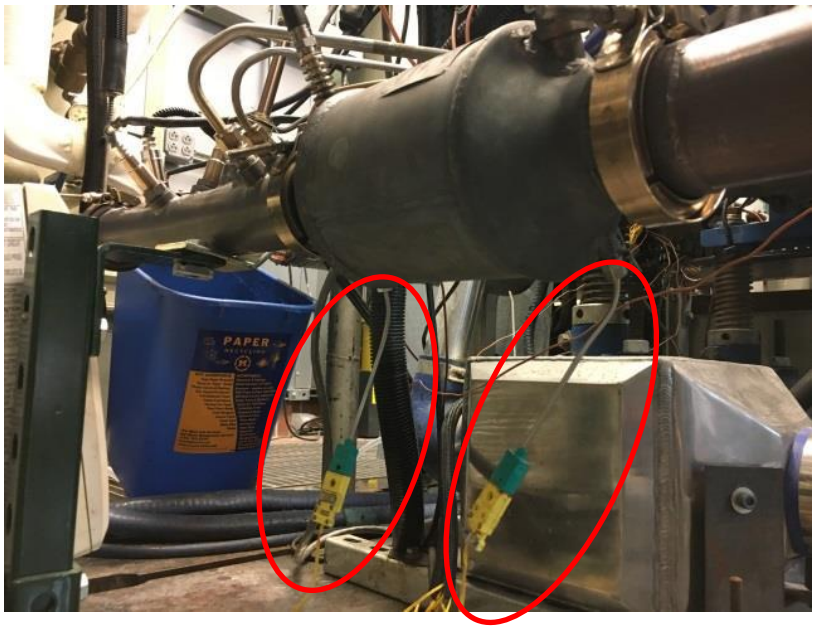

Figure 27: Thermocouples applied on the GPF.

T_e was kept constant around 400 °C during the soot accumulation phase of the tests with the use of a cooling system made of a fan, which cooled the GPF and a water flow on the exhaust tube. This was necessary to avoid passive regeneration events that could happen at temperatures higher than 450 °C. During the regeneration phases, the cooling system was turned off.

The scale was used at the end of each phase to evaluate the weight of the filter to determine how much soot was accumulated on the filter after the loading phase. Before starting with the experiments, the scale was calibrated. Together with the weight also the temperature of the filter was measured, because a temperature normalization process was performed (the weight procedure and temperature normalization are described in Appendix A).

Figure 28: Scale used to weigh the filter.

The Radio Frequency sensor used is provided by Amphenol [31], and a picture is showed in Figure 29.

Figure 29: Amphenol RF soot sensor [31].

The Radio Frequency sensor used for the experiments is provided with two antennas, one positioned at the inlet and the other at the outlet of the monolith. In Figure 30 a picture of the actual configuration antennas/filter is presented. Even if the position (inlet/outlet) of the antennas should not influence the signal, they were always mounted in the same location.

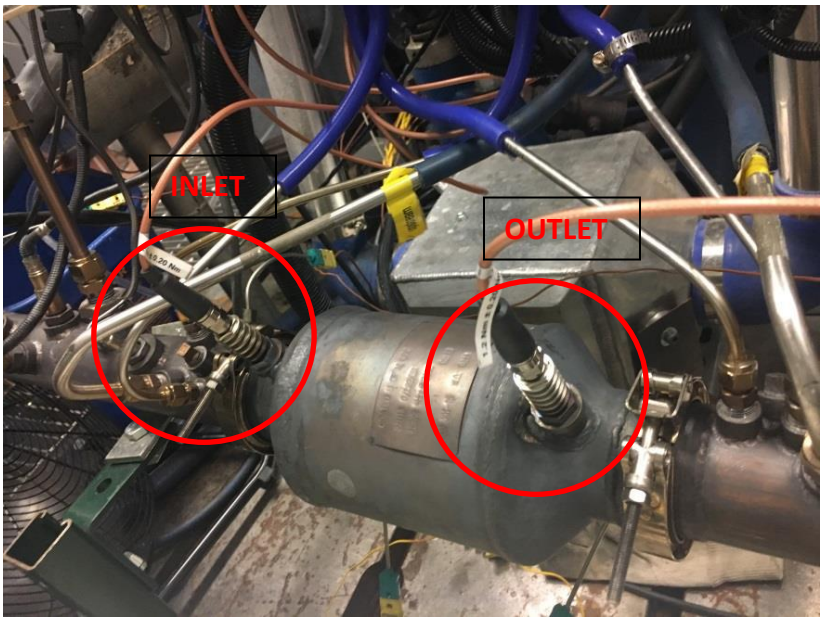

Figure 30: RF sensor antennas.

When the engine ran, the sensor data was collected through RealTerm, a software installed on the laboratory computer, which transmits a vector of data elements following each of its measurements. The transmitted data are ASCII characters separated by a comma.

Table 5 shows the different types of data that the sensor sends via serial communication interface. Data element number three, which is the average forward gain, is the parameter chosen as a sensor output for easy review of the soot amount loaded in the filter.

Table 5: Data elements available via serial communication interface [31].

Data Element	Name	Values
1	RESERVED	Reserved for future use. Appear as “INVALID” string.
2	RESERVED	Reserved for future use. Appear as “INVALID” string.
3	S21AVG	Average Forward Gain calculated over all frequency bins (units of dB)
4	S21 Sd Dev	Standard deviation of forward gain calculated over all frequency bins (units of dB)
5	RESERVED	Reserved for future use. Appear as “INVALID” string.
6	RESERVED	Reserved for future use. Appear as “INVALID” string.
7	RESERVED	Reserved for future use. Appear as “INVALID” string.
8	RESERVED	Reserved for future use. Appear as “INVALID” string.
9	Noise Measurement	Received power level measured with no RF signal generated by the sensor module
10	Noise Floor	Received power level during factory calibration + 3 dB
11	Min Received Power	Smallest received power observed during measurement sweep across all frequency bins
12	Noise Threshold	Smallest received power observed during measurement sweep across all frequency bins – 3 dB
13	HW Status	Zero if valid factory calibration data available or else Oxff=255
14 - 214	Forward Gain Frequency Array	200 element array of forward gain measurement (units of dB) calculated at each frequency bin (2.1,2.1005,…,2.2 GHz)

The sensor operates in the frequency range between 2.1 ÷ 2.2 GHz; the forward gain (dB) is calculated each 0.5 MHz, every 10 s (Radio Frequency sensor sampling frequency) using the information of power value at the outlet and inlet antennas. It is evaluated by the sensor control unit in this way:

Equation 4: Forward Gain formula used by the Radio Frequency sensor.

$$Forward\ Gain\ (dB) = 10 \log_{10} \frac{P_o}{P_i}$$

In Figure 31 an example of plot of the forward gain as a function of the frequency range is shown for the initial moment of the loading phase, as an example of the typical trend.

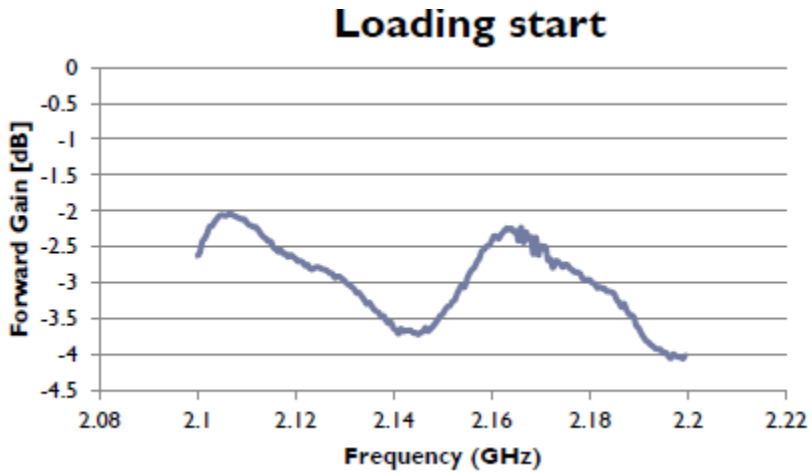

Figure 31: Plot of the first vector of Forward Gain vs. frequency, in a GPF loading case.

The average forward gain is evaluated as the average of all the forward gains, each 10 s by the control unit of the sensor.

3.2 Test procedure

The normal operations a GPF performs during its life are:

- Soot accumulation (Loading phase);
- Soot burning (Regeneration phase).

In this study, they have been explored using a standard test procedure made up of the following subsequent events:

1. Clean Regeneration;
2. Soot accumulation (called from now on loading);
3. Loaded Regeneration.

The test starts with a soot-free filter which undergoes regeneration conditions (Clean Regeneration), then the engine is run for a defined time so that the GPF is loaded with a certain amount of soot (Loading), and finally the filter is regenerated, and all soot present is oxidized (Loaded Regeneration). In one of the tests, deceleration fuel shut off (DFSO) event was also explored; the regeneration was normally started and then the fuel was cut off to simulate the interruption of fuel injection in case of deceleration. In this way, it is also possible to simulate the Radio Frequency sensor response when the regeneration event is suddenly interrupted.

As final test, a different procedure was followed to have more information on the soot loaded during the cycle. This process, called from now on “final test” is described after the standard procedure test. Both procedures have been performed with coated and uncoated filter.

3.2.1 Clean Regeneration

Clean regeneration was performed at the beginning of the standard test cycle, when the filter was clean. In this event, no soot was present on the filter. The effects of regeneration temperatures on the signal of the sensor could be noticed, and it was sure that all the possible residual soot was completely oxidized.

The steps followed, after the engine was turned on, to achieve the regeneration conditions were:

1. Engine warm up: 1200 rpm @ 4 bar, until the temperature of the coolant reaches 80 °C;
2. Baseline condition: 1600 rpm @ 8 bar, until the T_e at the inlet of the monolith reaches 430 °C ;
3. Regeneration condition: 2000 rpm @ 12 bar for a total time of 30 minutes.

In Table 6 engine operating conditions set during clean regeneration event are summarized.

Table 6:Clean regeneration engine operating conditions.

Operating conditions	Engine speed [rpm]	BMEP [bar]	SOI [°BTDC]	INJ Pressure [Mpa]	Duration [hr]
Clean Regeneration	2000	12	285	6	0.5

When the clean regeneration phase ended, the following steps were performed:

- The engine was shut off;
- The GPF was dismounted from the exhaust system;
- The GPF was weighed on the scale when it is hot (~130 °C)
- The GPF was cooled down;
- The GPF was weighed again when it is cold (~100 °C);
- The GPF was re-mounted in the exhaust system.

In this procedure, the GPF has been weighed at two different temperatures because it is necessary to consider that when it cools down soot absorbs water. For this reason, a temperature normalization is performed, described in Appendix A .

Then, the loading phase is initiated.

3.2.2 Test conditions (Loading)

After the clean regeneration, the engine is run to accumulate soot on the filter.

In parallel with this work, a PhD student at the University of Michigan has investigated soot reactivity at different operating conditions. It has been demonstrated that varying the engine operating parameters (Start of Injection, Injection pressure) soot reactivity changes, meaning that a different oxidation timing is necessary to completely oxidize the soot accumulated in the filter.

According to the abovementioned study, Figure 32 shows how the mass of soot oxidized changes as a function of time, for different injection conditions. It is evident that changing the injection timing or the injection pressure affects the reactivity of the soot.

Since this thesis aims to determine if it is possible to detect the differences in the soot reactivity, the three cases “Early Start Of Injection”, “Late Start Of Injection” and “Low injection pressure” were chosen as loading characteristics of the tests performed. Early SOI conditions determine the formation of the least reactive soot, hence the soot that needs the major time to be completely oxidized. Reactivity in late SOI and low injection pressure is similar, and higher with respect to early SOI, so that less time is required to oxidize the soot.

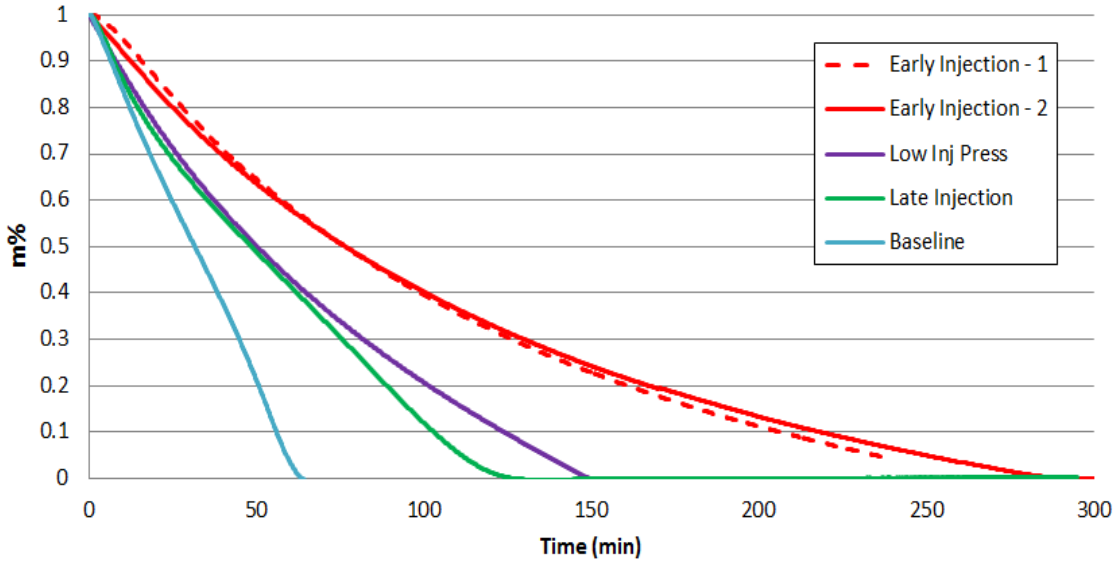

Figure 32: Mass of soot oxidized vs. time for different engine operating conditions.

The difference in soot reactivity is not detectable with the differential pressure sensor; since soot reactivity is an important parameter to determine the regeneration duration, one aim of this research is to find if the Radio Frequency sensor is capable of perceiving this difference.

Again, after the engine was turned on, the following conditions were set:

1. Engine warm up: 1200 rpm @ 4 bar, until the temperature of the coolant reaches 80 °C;
2. Baseline condition: 1600 rpm @ 8 bar, until the T_e at the inlet of the monolith reaches 430 °C;
3. The injection condition is set.

Table 7 summarizes the engine parameters for the three different chosen loading conditions:

Table 7: Engine operating parameters for the three different loading conditions.

Operating conditions	Engine speed [rpm]	BMEP [bar]	SOI [°BTDC]	INJ Pressure [Mpa]
Early SOI	1600	8	325	6
Late SOI	1600	8	150	6
Low injection pressure	1600	8	285	2
Stock	1600	8	285	6

The amount of soot to be accumulated is set to 2 g/l as maximum value, not to damage the filter. The duration of the loading phase was chosen based on the different injection conditions, because of the different soot emission rate. Figure 33 presents the different clack carbon soot concentration in soot produced in the four different operating conditions. On the basis of this experimental result, the duration of each test was defined.

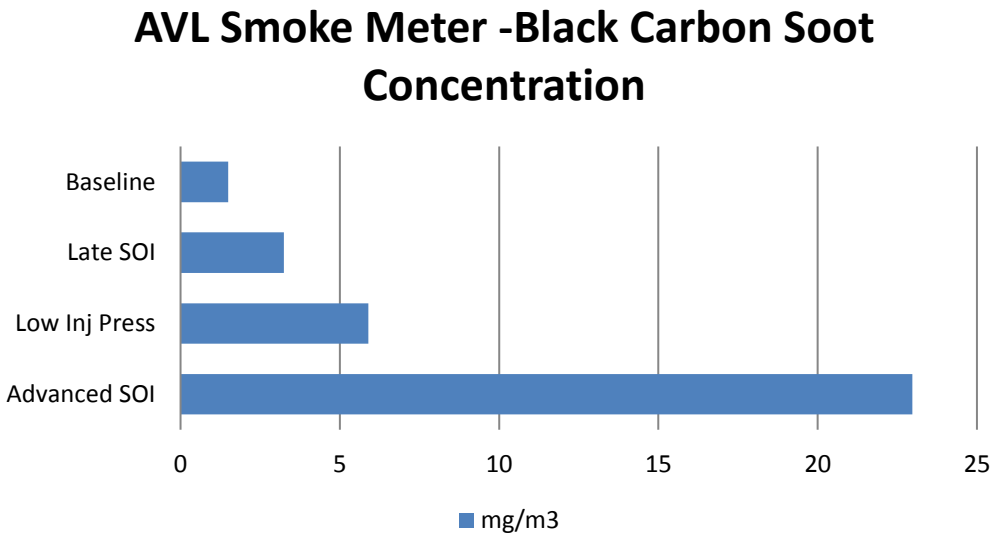

Figure 33: Black carbon soot concentration of soot produced in the four different operating conditions.

The duration of the tests in shown in Table 8:

Table 8: Loading operating conditions with relative duration

Operating conditions	Duration [hr]
Early SOI	~ 1.5
Late SOI	~ 7
Low injection pressure	~ 4.5

At the end of the loading phase, the procedure described previously at the end of the 3.2.1 Clean Regeneration paragraph is performed again:

- The engine is shut off;
- The GPF is dismounted from the exhaust system;
- The GPF is weighed on the scale when it is hot (~130 °C)
- The GPF is cooled down;
- The GPF is weighed again when it is cold (~100 °C);
- The GPF is re-mounted in the exhaust system.

The last step is the filter regeneration.

3.2.3 Filter Regeneration

The last phase of the standard test was the filter regeneration. During this phase, all soot accumulated during loading was oxidized and the GPF returned to be clean. To be sure that all soot was oxidized after the regeneration conditions were reached (2000 rpm @ 12 bar of BMEP) the loaded regeneration lasted 1 hour.

In Table 9 the engine operating conditions for the filter regeneration phases are summarized:

Table 9: Engine operating conditions during filter regeneration phases.

Operating conditions	Engine speed [rpm]	BMEP [bar]	SOI [°BTDC]	INJ Pressure [Mpa]	Duration [hr]
Filter Regeneration	2000	12	285	6	1

3.2.4 Final Test

The last test was performed following a different procedure:

1. Warm up of the engine (1200 rpm @ 4 bar);
2. Baseline condition (1600 rpm @ 8 bar);
3. Change of injection conditions;
4. Constant operating conditions for 25 minutes (soot accumulation);
5. Engine was turned off;
6. GPF was dismounted and weighed at hot and cold temperatures (Appendix A for weighing procedure);
7. GPF was mounted again in the exhaust system.

All these steps were repeated three times, to have four different gravimetric measurements of the soot accumulated on the filter during the all test. This test was performed one time at early SOI conditions; the operating conditions are presented in Table 10:

Table 10: Final test engine operating conditions.

Operating conditions	Engine speed [rpm]	BMEP [bar]	SOI [°BTDC]	INJ Pressure [Mpa]	Duration [min]
Early SOI	1600	8	325	6	25

4. EXPERIMENTAL RESULTS

The procedure described in 3.2 Test procedure was performed for both uncoated and coated filter. However, only data obtained from the uncoated filter testing were processed for the creation of the model. In this way, the influence of the catalyst was avoided. In total, five tests were performed for the uncoated filter:

1. Three tests at early SOI (385 °BTDC) (Test 1, Test 2 and Final Test);
2. One test at late SOI (165 °BTDC);
3. One test at low injection pressure (2 MPa);

At the end of each test, the average forward gain obtained from the sensor as output was plotted as a function of time. As preprocessing, together with the Radio Frequency output signal also the T_e and DPS signal were analyzed and time aligned with RF data. As first step the data from the Radio Frequency sensor and the T_e at inlet and outlet were time aligned. That was possible because a sharp change in the T_e determines a change in Radio Frequency sensor response. All the graphs were visually checked and the discussion is reported in this chapter, referring to the different phases of the test described in the methodology section.

Even if only data from the uncoated filter have been processed, in this section a brief comparison between the raw data from both types of filter will be presented, first for the standard tests and then for the final test.

4.1 Raw data discussion

Based on the working principle knowledge of Radio Frequency sensor, when the soot is accumulated on the filter, the output signal (average forward gain) is attenuated following a linear trend [37]. When the loading data were analyzed, this was found to be true for the coated GPF as shown in Figure 34. The figure presents the average forward gain trend as a function of time for the early SOI loading conditions and it is possible to notice that as far as the soot amount in the filter increases the value of the average forward gain linearly decreases, indicating that a univocal correlation exists between the two parameters.

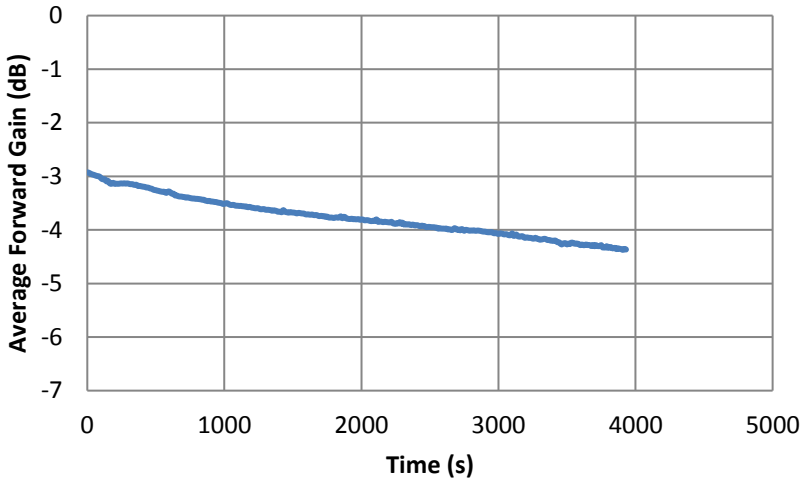

Figure 34: Average forward gain as a function of time, captured for early SOI conditions, in the case of the coated filter.

In the case of uncoated filter tests, the RF output plots presented a different trend, which was not in accordance with the literature [37]. In fact, the trend of the average forward gain is not linear, but parabolic. This means that there is not a univocal correlation between the average forward gain and the soot amount in the filter. Indeed, at the beginning of the test the Radio Frequency output signal increases, and then it starts its decreasing trend. In Figure 35 the Radio Frequency sensor output from the early SOI test for the uncoated GPF is presented:

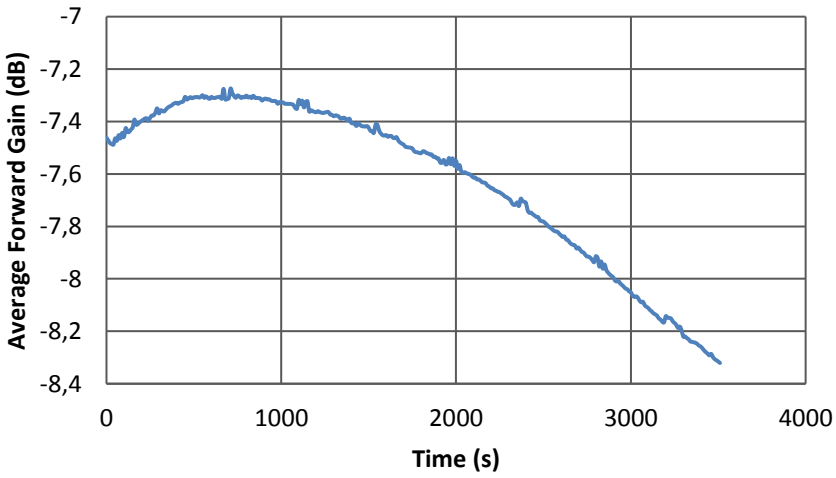

Figure 35: Average forward gain as a function of time, captured for early SOI conditions, in the case of the uncoated filter.

As mentioned in the methodology paragraph, the average forward gain is considered in this study as the output parameter of the sensor to be correlated to the accumulated amount of soot. However, the average forward gain is evaluated by the sensor electronic control unit every ten seconds as the mean value of the forward gains at each frequency bin $(2.1, 2.1005, \dots, 2.2\ GHz)$. It was decided to check the single forward gain values, plotting them as function of the frequency range at different time points of the experiments to determine the frequency range to be used for this application.

Forward gain values were plotted the outcome is shown in Figure 36:

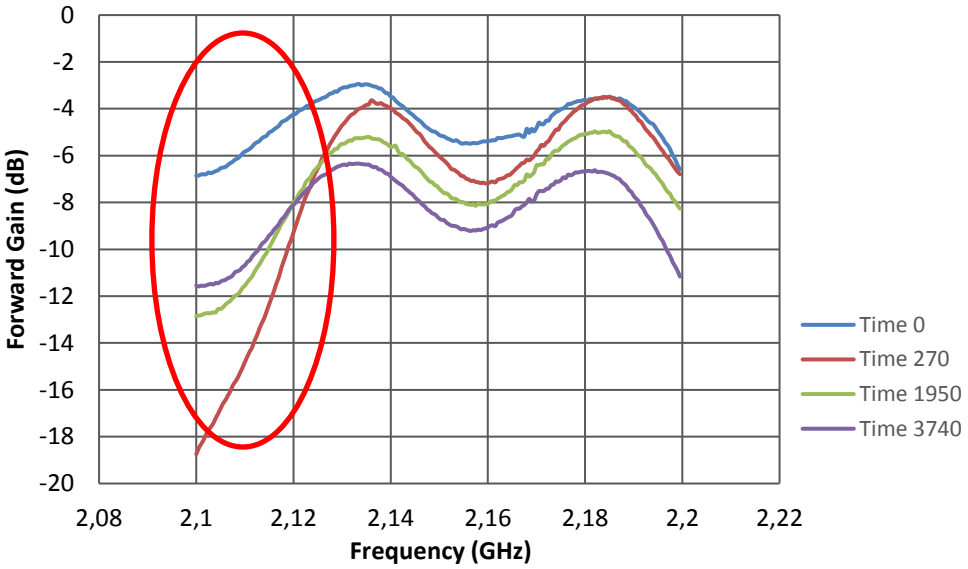

Figure 36:Forward Gain vs. Frequency at different time instant during early SOI loading test of uncoated filter.

In Figure 36 each curve shows two peaks, one at low frequency and the other at high frequency. These frequency values represent the resonance frequency, which is reduced as soot accumulates in the filter. This follows what was specified in literature [38]. The problem was identified in the part of the curves that is before the low frequency peak (circled in red in Figure 36), because it is in contrast with the rest of the curve, which shows forward gain that increases with soot accumulation. Since these values are used by the Radio Frequency sensor control unit to evaluate the average forward gain, the result is the distorted signal shown in Figure 35. This can be explained saying that the RF sensor was used for diesel particulate filters and off-road filters (which could capture up to 100 g of soot) applications, and these filters have different

geometry and dimensions respect to GPFs. Consequently, not the all frequency range is suitable for GPF application. All the forward gain values correspondent to frequencies lower than the first resonance frequency were removed, using Matlab. In the next pages the postprocessed Radio Frequency sensor output trend obtained for the uncoated filter are presented.

4.2 Standard Test - Clean Regeneration

Clean regeneration is the first phase of the standard test procedure. After the engine is warmed up, it is run for 30 minutes at constant speed and load in the regeneration conditions (2000 rpm @ 12 bar of BMEP) as reported in the paragraph 3.2.1.

Results from the Radio Frequency sensor signal aligned with the temperature trend for the uncoated GPF are reported in Figure 37:

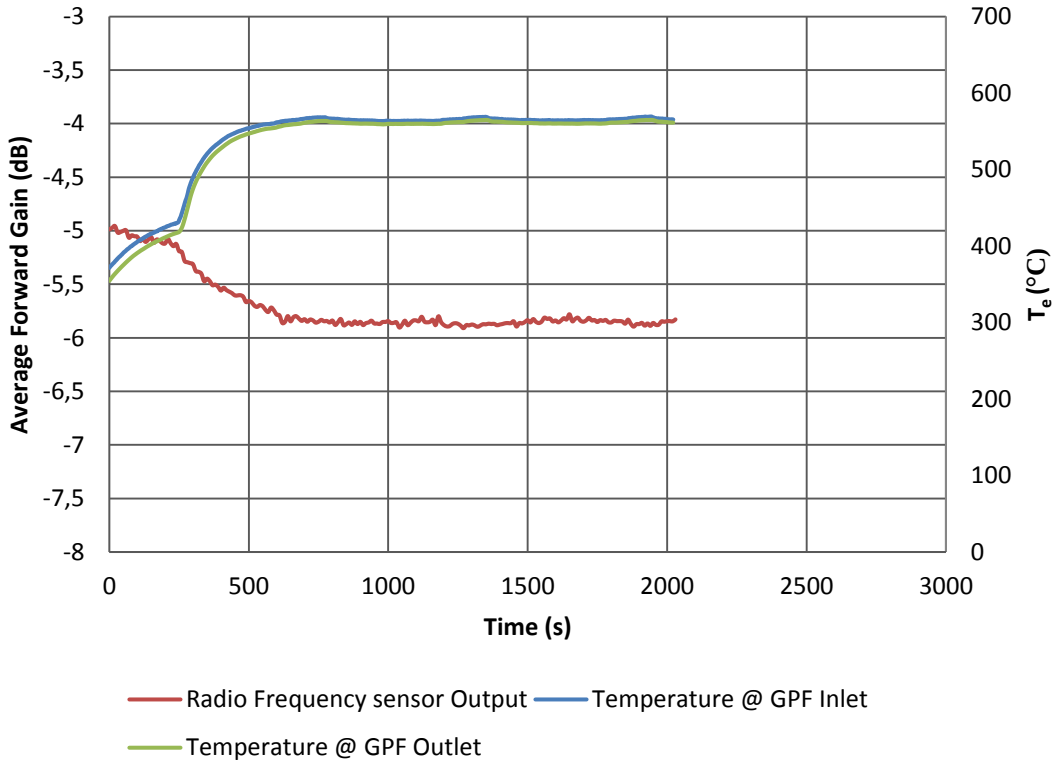

Figure 37: Trend of T_e at inlet and outlet of the GPF and Radio Frequency sensor output vs. time during clean regeneration for the uncoated filter.

The same results for the coated filter are shown in Figure 38:

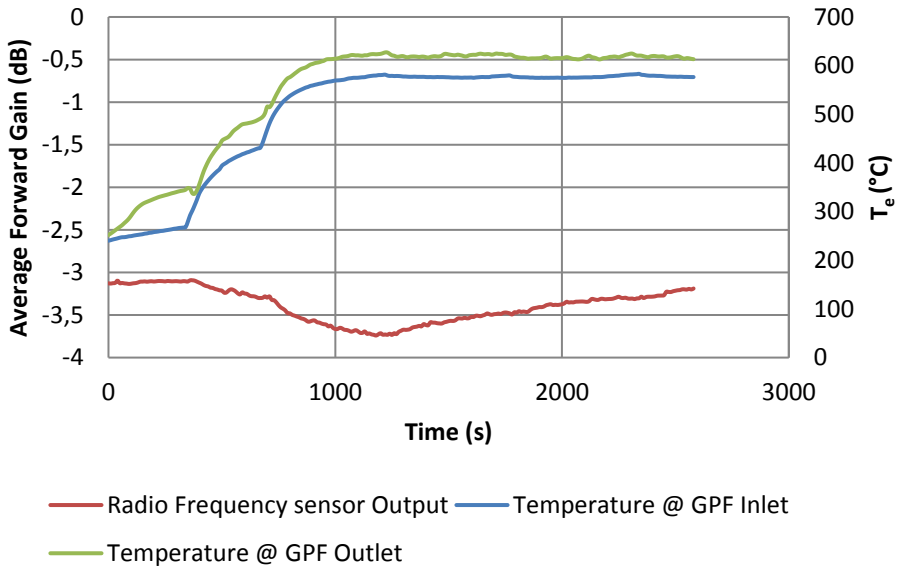

Figure 38: Trend of T_e at inlet and outlet of the GPF and Radio Frequency sensor output vs. time during clean regeneration for the coated filter.

As it is evident Radio Frequency sensor gives a different output for the two different filters. During clean regeneration, there is no soot present in the GPF, whereas temperature increases during the whole process until it becomes steady. In Figure 37, for the uncoated filter, the signal is attenuated by the increase of temperature; an attenuation of 1 dB is due to 200 ºC variation in the temperature. In this case T_e at the inlet and outlet of the GPF is approximately the same, since no reactions happen inside because the filter is uncoated. On the other hand, in Figure 38 obtained from the coated GPF testing, the signal is less affected by temperature. In the last part of the signal when temperature is higher than 500 ºC, the trend increases due to residual soot that is oxidizing. It is also worth noticing that the average forward gain range is different in the two cases: in the former case the drop is from -5 dB to -5.8 dB, whereas in the latter case the signal varies in the range from -2 dB to -3 dB. This difference is due to the presence of the catalyst. This difference shows up also in the other phases of the tests.

At the end of the clean regeneration, the filters are dismounted and weighed on the scale.

4.3 Standard Test - Loading

The loading case started again with engine warm up. When the temperature of the coolant reaches 80ºC, the user changes engine parameters to set loading conditions (1600 rpm @ 8 bar BMEP). When operating conditions get stable, start of injection or injection pressure was changed to the defined test conditions. In the Early SOI case loading phase was set at 1 hour, as time necessary to collect ≈2 g/l (3.8 g) of soot. This value was chosen because it is the soot threshold value not to damage the filter.

Firstly, graphs are presented for the uncoated filter and then for the coated filter.

4.3.1 Early SOI

The results from the early start of injection loading (385 ºBTDC) are now discussed.

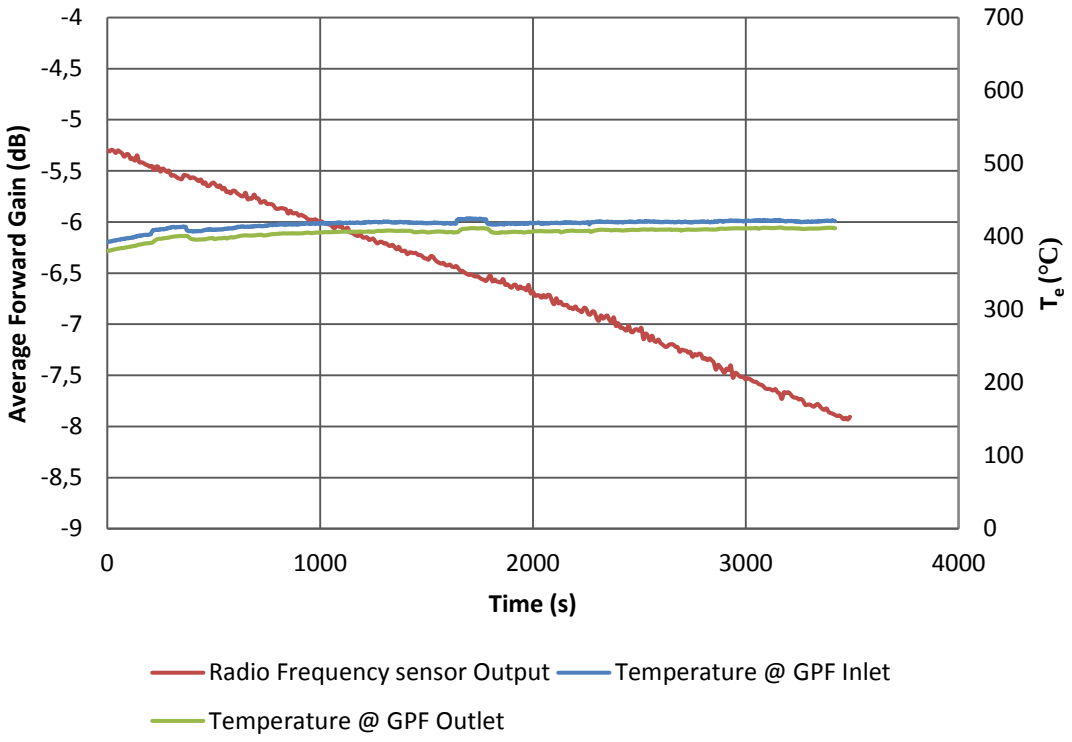

Figure 39:Trend of T_e at inlet and outlet of the GPF and Radio Frequency sensor output vs. time early SOI loading for the uncoated filter.

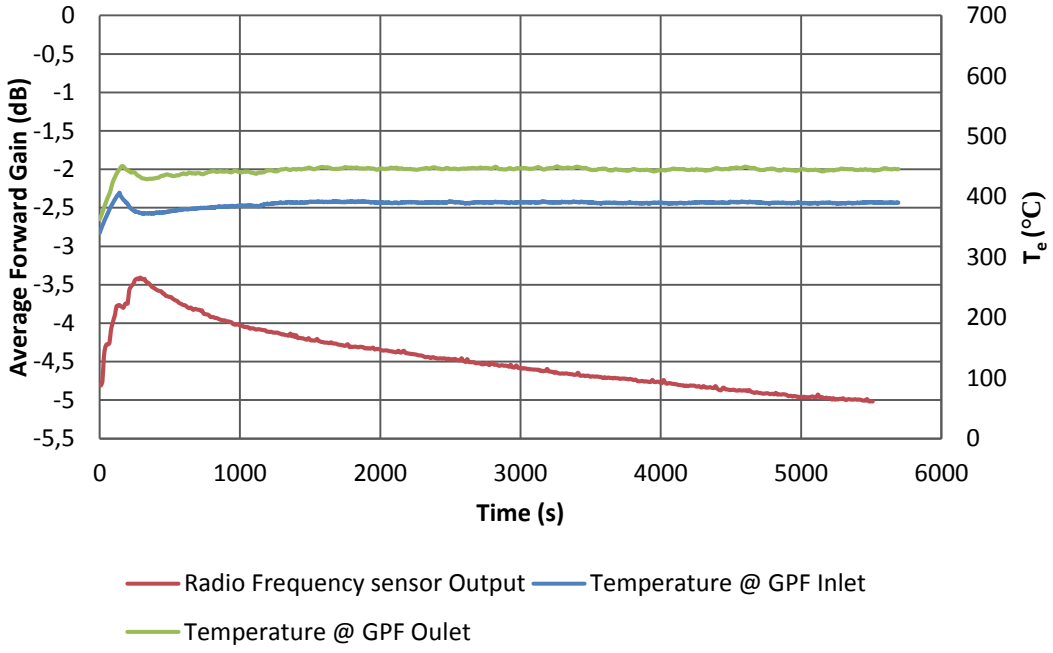

Figure 40: Trend of T_e at inlet and outlet of the GPF and Radio Frequency sensor output vs. time early SOI loading for the coated filter.

From this results it is possible to notice that the average forward gain in the two cases follows a linear trend. In the case of the uncoated filter, in Figure 38, T_e is constant during the entire process.

In Figure 39, in the case of coated filter, there is a small increase at the beginning due to the rapid increase of T_e and absence of soot. Then, the cooling system was turned on and T_e stabilizes, RF output starts to decrease almost linearly with soot accumulation.

4.3.2 Late SOI

As second case, the results from late SOI (185 ºBTDC) are presented. In this case, it was necessary to run the engine for a longer time (≈ 7 hours) to get the same amount of soot as early SOI case.

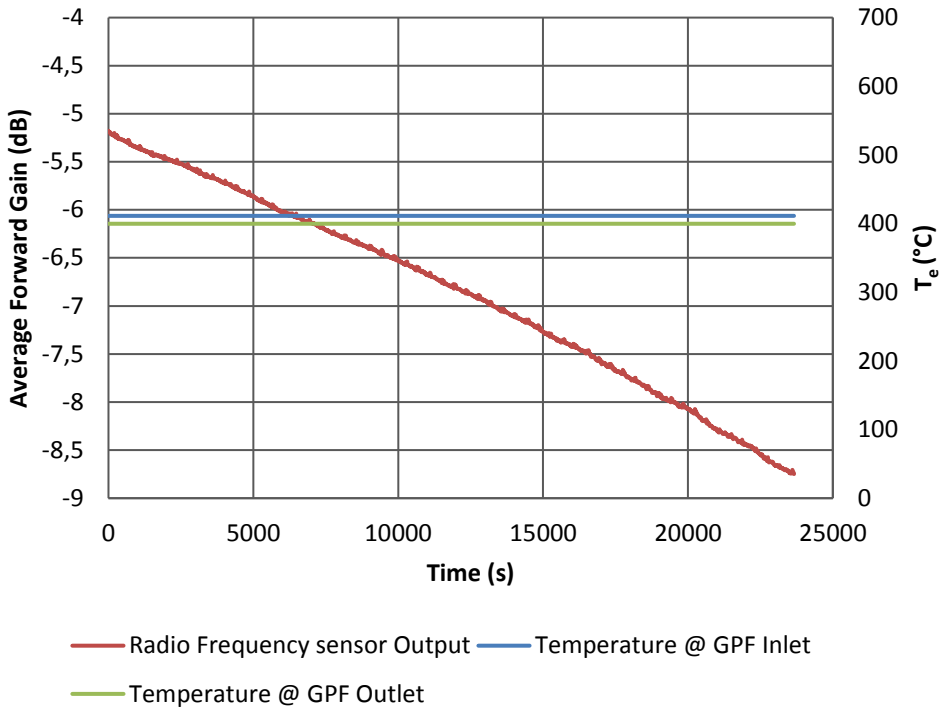

Figure 41: Trend of T_e at inlet and outlet of the GPF and Radio Frequency sensor output vs. time late SOI loading for the uncoated filter.

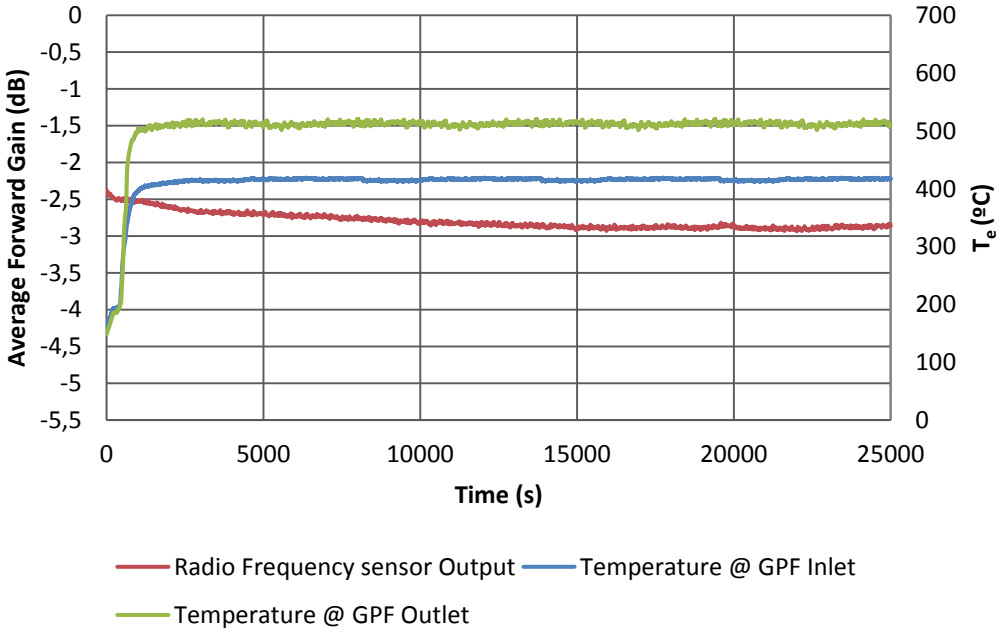

Figure 42: Trend of T_e at inlet and outlet of the GPF and Radio Frequency sensor output vs. time late SOI loading for the coated filter.

Again, in Figure 41, with the uncoated GPF the Radio Frequency output trend is linear. Temperature is constant around 410 ºC, and only soot causes the attenuation of the signal.

The late SOI injection test created some troubles with the coated filter. Exhaust temperatures in the late SOI case are higher due to high unburned HCs for this case, as it is visible in Figure 42. Due to the presence of the catalyst in the coated GPF, T_e at the outlet is very high and, these high temperatures combined with the slow slope of the Radio Frequency signal attenuation, suggested that some regeneration may be happening in the meanwhile. The cooling system may not lower the temperature enough to allow a correct accumulation of soot. Hence, in this case soot is produced and some is oxidized immediately after.

Again, at the end of each loading phase weights measurements were taken. In Table 11, the results from the weight procedure are shown both for the clean filter and the soot loaded filter.

Table 11: Clean filter, Soot loaded filter weights and amount of soot accumulated during the loading phases.

Injection conditions	Clean filter	Soot loaded filter	Soot loaded
Early SOI	2201.2 g	2203.7 g	2.5 g
Late SOI	2201.2 g	2203.7 g	2.5 g
Low injection pressure	2202.2 g	2204.1 g	1.9 g

Filters were weighed twice, at high temperature (≈130°C) and low temperature (≈100°C) because it was necessary to perform a temperature normalization. Each time multiple measurements were taken, and then the average weight was considered if the standard deviation value was acceptable (weighing procedure description is present in Appendix A).

4.4 Filter Regeneration

Loaded regeneration is the most interesting phase of the entire test. In fact, soots produced in the different operating conditions were shown to have different reactivity, and it was worth to notice if Radio Frequency sensor is capable to distinguish this characteristic. The results for the early SOI soot produced are reported for both the coated and the uncoated GPF, and finally a

comparison between the regeneration for the different operating conditions is presented for the uncoated filter.

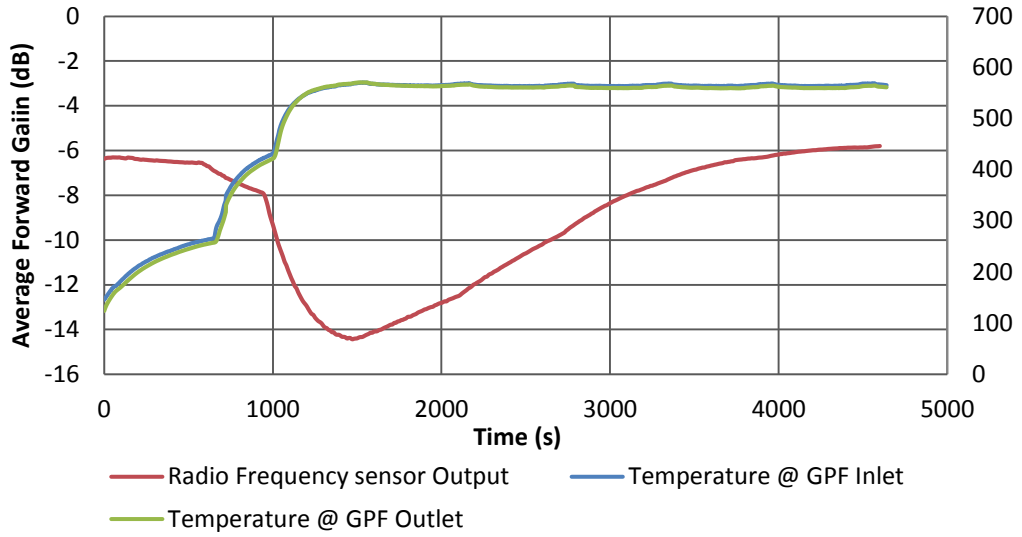

Figure 43: Trend of T_e at inlet and outlet of the GPF and Radio Frequency sensor output vs. time of early SOI soot produced regeneration for the uncoated filter.

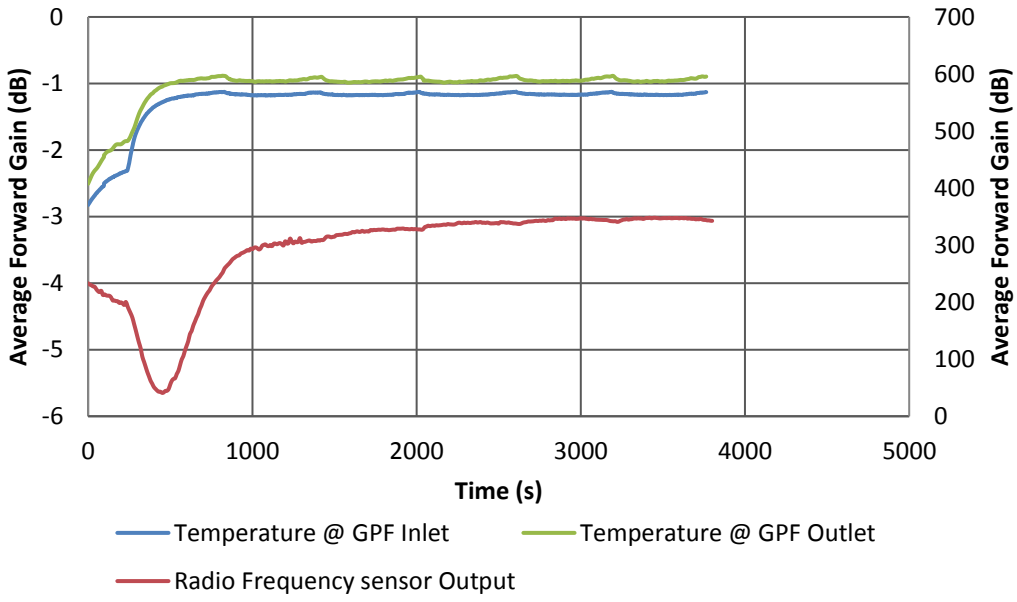

Figure 44: Trend of T_e at inlet and outlet of the GPF and Radio Frequency sensor output vs. time of early SOI soot produced regeneration for the coated filter.

Firstly, just watching at the Radio Frequency output signal in Figure 43 and Figure 44 it is understandable that soot oxidizes faster in the catalyzed filter, as expected.

Soot starts to burn around 500 ºC; as soon as T_e reaches that value the average forward gain begins to grow. When signal is constant, it is deductible that no more soot is present in the filter. Regeneration time is set to one hour to be sure that all soot present in the filter is completely oxidized, but in the case of coated GPF this time is much overestimated, since the Radio Frequency signal remains stable for a long time. According to this result, regeneration time may be optimized by further studying Radio Frequency sensor application.

Another interesting point to be underlined is the influence of the T_e before it get stable:

- Temperature range 100 ºC ÷ 260 ºC: Radio Frequency signal is not affected by temperature change and remains constant;
- Temperature range 260 ºC ÷ 430 ºC: Radio Frequency signal is attenuated. In fact, soot is a dielectric material, and its conductive properties change with temperature. This attenuation is then due to increase conductivity of soot. This result matches what found in literature for a DPF [38].
- Temperature range 430 ºC ÷ 500 ºC: regeneration is not started yet, but the curve changes its slope. Probably temperature becomes more influencing at this point.
- Temperature range 500 ºC ÷ 570 ºC: soot starts to oxidize, but during this time Radio Frequency signal is affected both by temperature increasing and soot oxidation. Soot starts to oxidize slower and so the attenuation due to temperature effect is greater at the beginning. Then soot starts to oxidize faster, and the curve changes its slope to finally start growing.

In case of DFSO during the regeneration event, fuel was cut after regeneration conditions were about to be reached, and T_e dropped down, so that soot oxidation was suddenly interrupted. Then the regeneration conditions were established again. In Figure 45 the trends of the T_e and the Radio Frequency sensor output are shown; notice that average forward gain strongly depends on temperature variation.

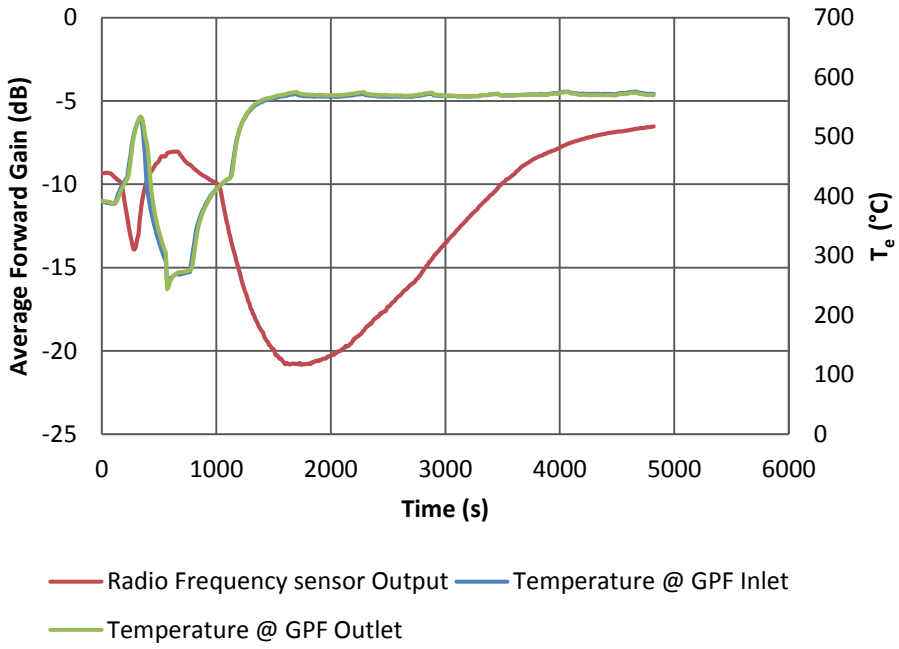

Figure 45: Trend of T_e at inlet and outlet of the GPF and Radio Frequency sensor output vs. time of early SOI soot produced regeneration with DFSO event for the uncoated filter.

To better understand the characteristics of the curves, the three regeneration curves obtained from the testing of uncoated GPF are superimposed. Moreover, the differential pressure sensor results for the same experiments are presented, to underline some advantages of Radio Frequency sensor.

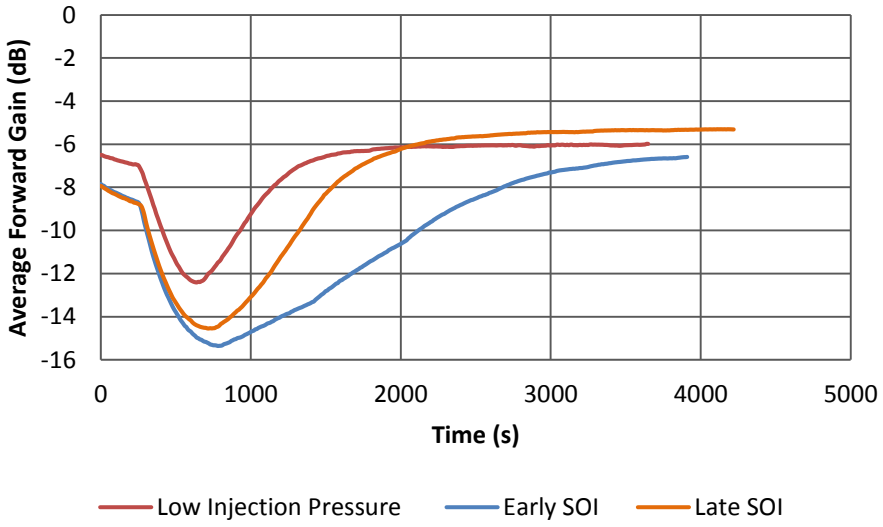

Figure 46: Comparison between regeneration phases of early SOI, late SOI and low injection pressure loading cases.

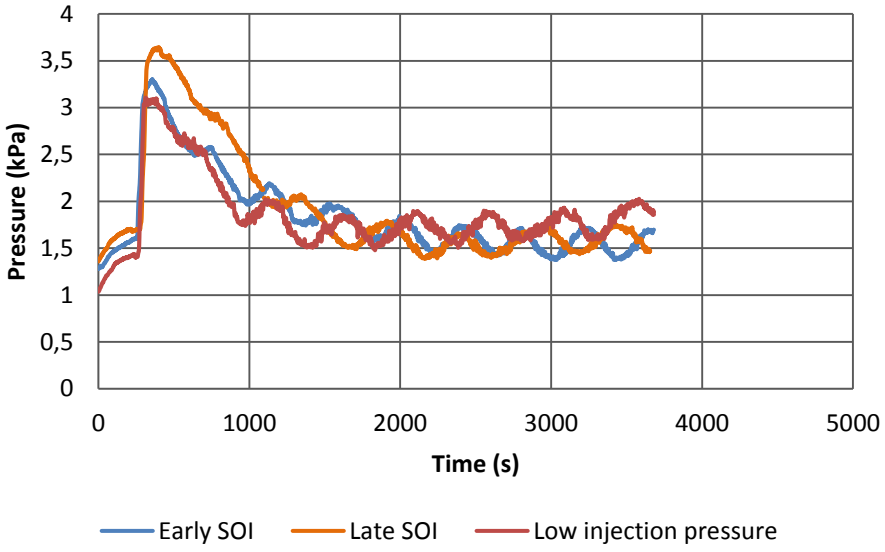

Figure 47: Differential pressure sensor output for early SOI (blue), late SOI (orange) and low injection pressure (red) test regeneration events.

The first thing to be underlined before analyzing Figure 46, is that the amount of soot accumulated during the loading phases was not the same for the three tests. In Table 12 the values are reported:

Table 12: Soot quantities accumulated in the early SOI, late SOI and low injection pressure loading cases.

Early SOI	Late SOI	Low Injection Pressure
2.5 gr	**2.5 gr**	**1.9 gr**

The first difference between the two sensors output is the “cleanliness” of the signal: differently from DPS signal in the RF case the trend is very defined and not noisy.

One important outcome of this comparison is the very defined distinction between the oxidation rate of soot for the three different operating conditions. In fact, as mentioned in the paragraph 3.2.2 according to Figure 32, soot produced in early SOI conditions is expected to be the slowest to burn. This distinction is hard or not possible to be detected from the pressure output of the differential pressure sensor shown in Figure 47, because the trends are among them very similar and they don’t show any peculiar characteristic related to differently produced soot. In fact, with DPS soot reactivity differences are not observable, since the

evaluation that DPS makes is an indirect measurement of the soot oxidation using information from other sensors (thermocouples, lambda sensor…), hence It is not an indicator of what is physically happening to the soot during the regeneration event.

From Figure 46 the following conclusions can be drawn:

- Early SOI: soot produced with these operating conditions is less reactive. This means that it needs more time to be completely oxidized. The curve does not reach a complete steady state, and the filter was not weighed so it is possible that not all the soot was removed from the filter. In fact, notice that the steady state value for the late SOI conditions is greater than early SOI one.
- Late SOI: this soot is evidently more reactive and the Radio Frequency output signal reaches a steady state value 1 hour of test, meaning that there are 20 excessive minutes of regeneration.
- Low injection pressure: in this case regeneration starts with a different amount of soot (1.9 grams); hence, the effect of the temperature in the attenuation of the signal is less, the minimum of the curve is ≈12 dB, against the ≈14 dB of the two previous cases. The steady state average forward gain value in this experiment is slightly lower than the late SOI value; this happened because steady state regeneration temperature was higher (385 °C).

4.5 Final test

This type of test was performed for two reasons:

- The filter was weighed three times during the test, then it was possible to have a rough trend of the soot accumulation;
- Two of the three total warm up phases were performed with some soot accumulated on the filter. Hence it would have been possible to study how temperature variation affects the signal when the filter is not clean. Unfortunately, all the Radio Frequency output during the warm up phases resulted to be very noisy and not reliable.

The Radio Frequency output is shown in Figure 48:

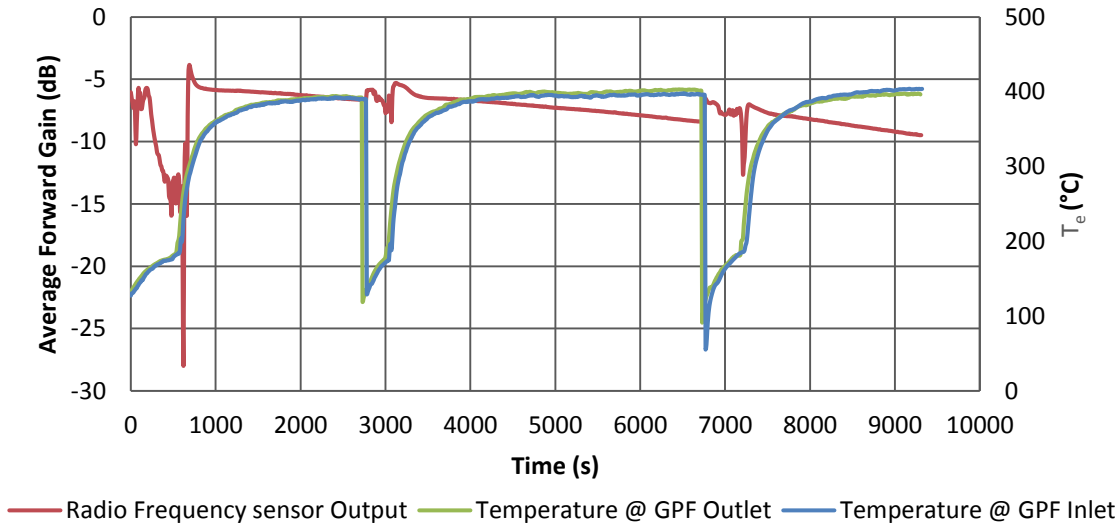

Figure 48: Final test Radio Frequency output and inlet and outlet GPF T_e trends as function of time.

During the warm up phases the signal is very noisy; even if it drops, as expected, with T_e increase, this transient values are not reliable to find a correlation with T_e. However, with this test four soot amount values were captured at the beginning, at the two temperature drop points and at the end. The approximate soot accumulation trend is reported in Figure 49:

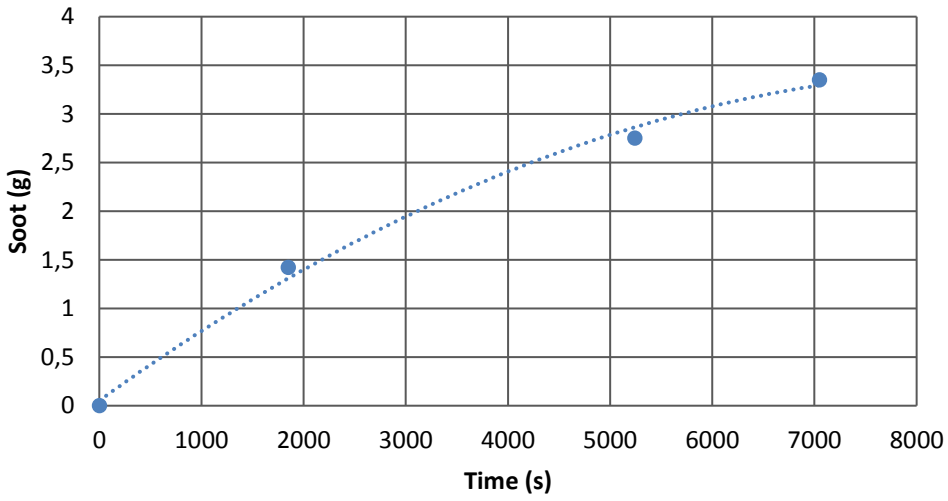

Figure 49: Trend of soot accumulation as function of time determined through the final test

4.6 Repeatability of experiments

To verify if the sensor use allows to have repeatable results, the early SOI test was repeated twice for the uncoated filter, with one-month time difference. From now on the two experiments will be referred as early SOI Test 1 and early SOI Test 2. Figure 50 reports the superimposed raw signals obtained in the loading phases:

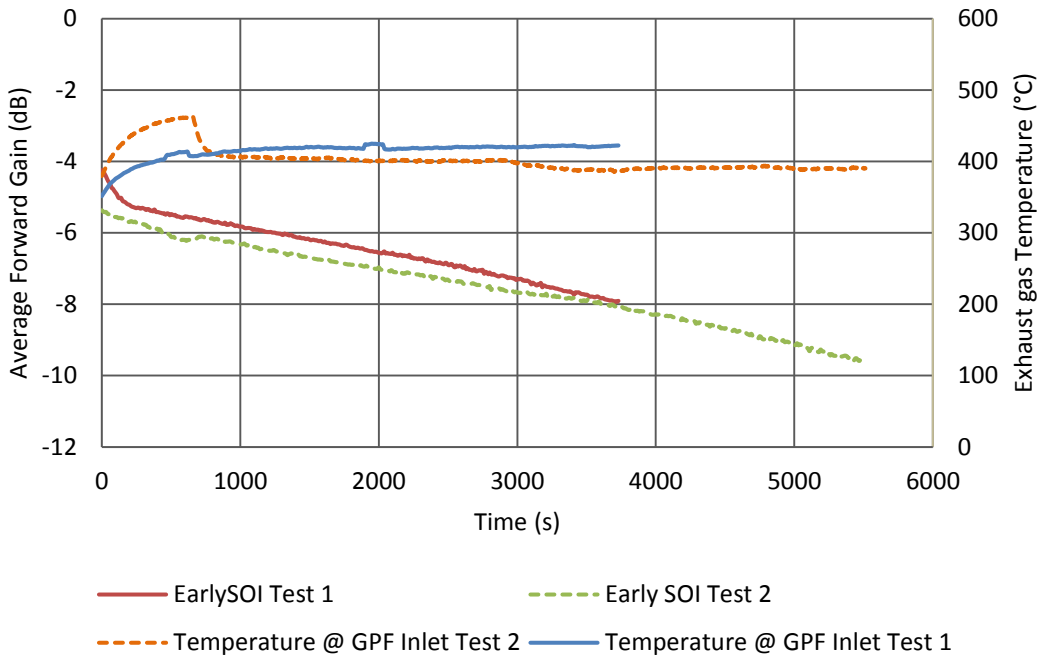

Figure 50: Comparison between two early SOI tests RF output and inlet GPF T_e.

Two observations need to be done:

- The two curves are parallel at the beginning, then the shift is caused by the difference in the T_e values;
- The dotted green curve slightly changes its trend due to the lowering of T_e in the last part of the experiment.

During the time between the two experiments, the GPF was cleaned and the antennas and thermocouples were dismounted and mounted again. These events could have negatively influenced repeatability of experiments. Instead, the two average forward gain curves result to be superimposed, and the experiment can be considered repeatable.

5. MODEL AND RESULTS

The aim of the data analysis is to create a model which correlates the three analyzed variables:

1. Soot accumulated (dependent variable);
2. Radio Frequency average forward gain (independent variable);
3. Temperature of the filter (independent variable);

The objective of modeling is to use the Radio Frequency average forward gain to estimate how much soot is present in the filter during loading and regeneration phases. Exhaust flow rate is another parameter that influences Radio Frequency signal according to literature [37], but experiments in this case were performed at constant operating conditions (rpm and torque), so it is not considered in the data processing. As far as temperature is concerned, no thermocouples are present to measure the actual temperature of the filter, so T_e at the inlet of the filter was used as approximation of that temperature.

A table listing the key points of the experiments was created, that was used to calibrate the model. To build the table it was assumed that soot accumulation during the warm up phases (when T_e increases) can be considered negligible, so that soot amount can be considered constant.

Two different approaches and two different datasets have been used for modeling the soot evolution during the loading and regeneration phases (the two tables with the dataset used for the two models are reported in Appendix B). For the loading phase, a surface fitting model on Matlab was used, whereas for the regeneration a multiple regression was found to be more appropriate for the soot oxidation phenomenon, because many combinations of the variables degree have been tried to determine the most representative.

The datasets were filled with average forward gain values correspondent to known amount of soot and correspondent T_e (0 g, 1.9 g, 2.5g, 2.75 g, 3.35 g). the very last point of the regeneration event in late SOI and low injection pressure tests were considered the soot-free filter points.

Soot loaded filter data were instead derived from the initial part of regeneration event dataset of late SOI test and low injection pressure test. In this way, it is possible to use the early SOI Test

1 dataset to validate the model, since the soot amount collected on the filter for this test is known. The final tables used to set the models are summarized in Appendix B.

5.1 Theory

The correlation between the three variables (average forward gain, temperature and soot amount) was determined using the multiple linear regression model. The general equation with multiple independent variables is reported in equation 1:

Equation 5: Multiple independent variables regression model [39].

$$y(n) = f(U, A) = \beta_0 + \beta_1 x_1(n) + \beta_2 x_2(n) + \cdots + \beta_n x_n(n) + \varepsilon$$

y is the dependent variable *n* is the number of independent variables and β_n are called regressor coefficients. The β_n values have to be determined to define the surface that represents the best approximation for the key points. To solve the equation and find the unknown parameters it is convenient to express the relation in matrix form:

$$Y = \begin{pmatrix} y_1 \\ \vdots \\ y_n \end{pmatrix} \quad U = \begin{pmatrix} 1 & x_{11} & x_{1k} \\ \vdots & \vdots & \vdots \\ 1 & x_{n1} & x_{nk} \end{pmatrix} \beta = \begin{pmatrix} \beta_1 \\ \vdots \\ \beta_k \end{pmatrix} \varepsilon = \begin{pmatrix} \varepsilon_1 \\ \vdots \\ \varepsilon_n \end{pmatrix}$$

The unknown coefficients are determined with the least squares method, so that the error ε is minimized [37]:

$$\varepsilon = ||Y - U\beta||^2 = \sum_{n=1}^{k} (y_n - f(u_n, \beta))^2$$

The solution β^* that minimizes the error is computed as [37]:

$$\beta^* = (U^T U)^{-1} U^T Y$$

In the specific case of this study, the Y vector is filled with the soot amount values listed in table 1, the independent variables are x_1, called from now on "T_e", and x_2, called from now on "Gain" which correspond to T_e and average forward gain values from the RF sensor, respectively.

At the end, the U matrix had this form:

$$U = \begin{pmatrix} {Gain_1}^{-1} & T_{e_1} & {T_{e_1}}^2 \\ \vdots & \vdots & \vdots \\ {Gain_n}^{-1} & T_{e_n} & {T_{e_n}}^2 \end{pmatrix}$$

This procedure has been exploited in two different ways in this thesis, once indirectly, using the surface fitting tool in MATLAB, and another time directly, computing the coefficient matrix β^* again in MATLAB. The first procedure was used to find an approximation for the loading event, the second was used for the regeneration event.

5.2 Model – Loading

All the data included in the Table 16 (Appendix A) were fitted with a polynomial surface using the curve fitting tool on MATLAB. Temperature values and average forward gain from the Radio Frequency sensor (two independent variables of the model) were given as input data, whereas the soot amount values were set as the output of the model (dependent variable). After the data were loaded in MATLAB, the order of each independent variable was set to determine a good approximation for the surface polynomial fitting.

To define the most appropriate order of the independent variables, firstly the soot values was plotted as a function of the correspondent average forward gain values (data listed in Table 16) at constant T_e values. From the result shown in Figure 51 it is possible to say that the trend of the soot as a function of the average forward gain at constant temperature has a parabolic shape. Consequently, it is necessary to consider a squared term of the average forward gain in the model.

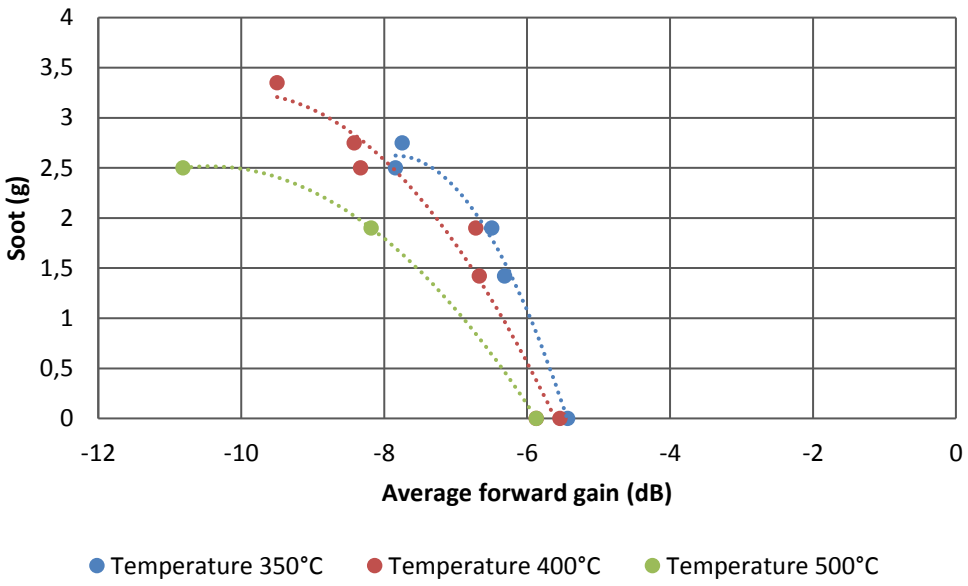

Figure 51: Soot amount as a function of average forward gain at constant temperature values.

About temperature influence, it is not possible to use the data in Table 16 to determine its relation with soot values at constant average forward gain values, so to start it was assumed to be linear.

Finally, the surface fitting obtained is shown in Figure 52:

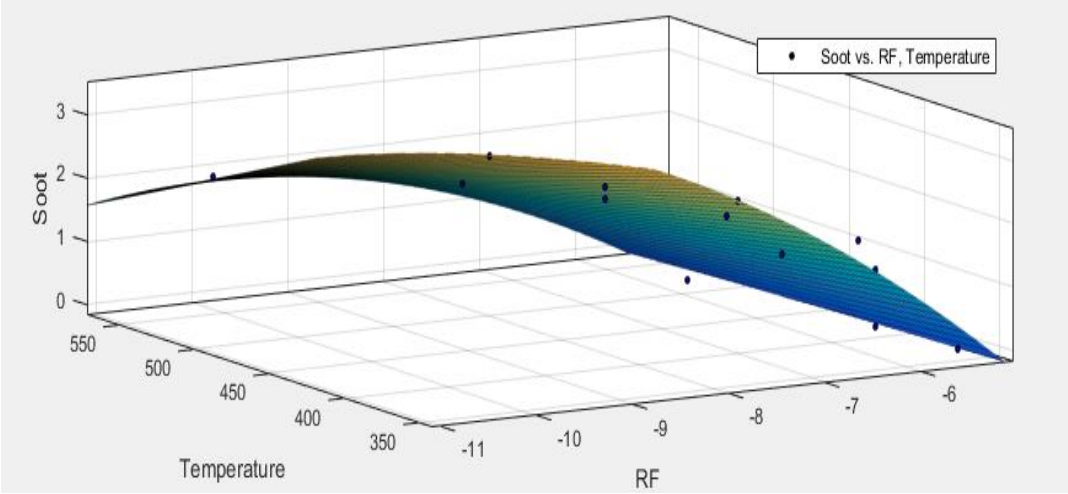

Figure 52: Surface fitting of key points, using Matlab curve fitting tool.

The polynomial approximation is of this type:

Equation 6: Analytical model which describe the soot accumulation phenomenon during loading phases.

$$Soot = a + b * RF + c * T_e + d * RF * T_e + e * RF^2$$

where RF is the average forward gain and T_e is the exhaust gas temperature at the inlet of the GPF. Together with the surface fitting, the curve fitting tool also provides the coefficient values of the polynomial equation which describes the surface (a, b, c, d, e). The surface fitting presents a R-square value of 95,64%. This model was then used for estimating the soot accumulation during loading phases. The results are presented in the paragraph 5.4.

All the dataset files with data collected from tests are organized like presented in Figure 53, and "RF" values and "Temperature" values were input to the model implemented in Matlab, to determine the soot evolution in time as output. The dataset is made of time dependent values of average forward gain and temperature values with a sampling frequency of 10 s. The soot evolution in time is not known, only the final value of soot accumulated was recorded as explained in the methodology section.

	A	B	C
1	Time	RF1	Temperature
2	0	-5.21417	370.493
3	10	-5.24253	372.185
4	20	-5.30342	373.956
5	30	-5.3531	375.793
6	40	-5.40984	377.027
7	50	-5.49537	378.15
8	60	-5.50833	379.493
9	70	-5.5007	380.813
10	80	-5.58689	382.211
11	90	-5.60365	383.671

Figure 53: Example of dataset retrieved from experiments.

5.3 Model – Regeneration

For the regeneration event, firstly using the curve fitting tool in MATLAB with different combinations of the independent variables degrees were evaluated. None combination was found to describe accurately the soot oxidation process, since temperature was not correctly compensated. In fact, the trend of soot during oxidation showed a peak at the beginning of the process which was caused by the temperature variation. To obtain the right temperature

compensation other key points were added to create the regeneration dataset (Appendix B), giving major information on the temperature transients.

Then instead of using the curve fitting tool on MATLAB, the multiple linear regression model, shown in 5.1 Theory was directly used for evaluating the coefficient matrix using MATLAB. During the regeneration event the soot evolution in time was unknown. For this reason, with an error and trial procedure many combinations of the two independent variables degrees were tried, considering both negative and positive degrees to find the best approximation for the soot oxidation phenomenon. The relation shown in Equation 7 was found:

Equation 7: Analytical model which describe the soot oxidation phenomenon during the regeneration phases.

$$Soot = a * RF^{-1} + b * T_e + C * {T_e}^2$$

For any positive degree of the average forward gain contribution the temperature was never enough compensated.

In the case of regeneration data processing, the high sampling frequency created some noise problems in the results obtained. Indeed, even if temperature was recorded with 1 ms sampling frequency, it was necessary to downsample it to 10 s to have correspondence between average forward gain from the sensor and T_e. On the other hand, during the engine operating condition changes, the T_e variations were very sharp, and with a high sampling frequency the derivative of the temperature have very sudden changes. When these values are input in to the model, they generated noise in the output signal, and to consider this limitation, a median filter was applied to the output signal of the model using the Matlab function "*medfilt1*".

5.4 Results – Loading

In this section, the model results for the both soot accumulation and oxidation trend only for the uncoated filter will be shown. Figure 54, Figure 55 and Figure 56 show the results for early SOI Test 1, late SOI and early SOI Test 2 in the case of loading phases, respectively. Soot amount is plotted as function of time. Then, the predicted values for the first two experiments are compared with measurements taken with the scale, and the error is evaluated. Notice that in the case of late SOI, the time needed to accumulate the defined amount of soot is much longer than in the case of early SOI.

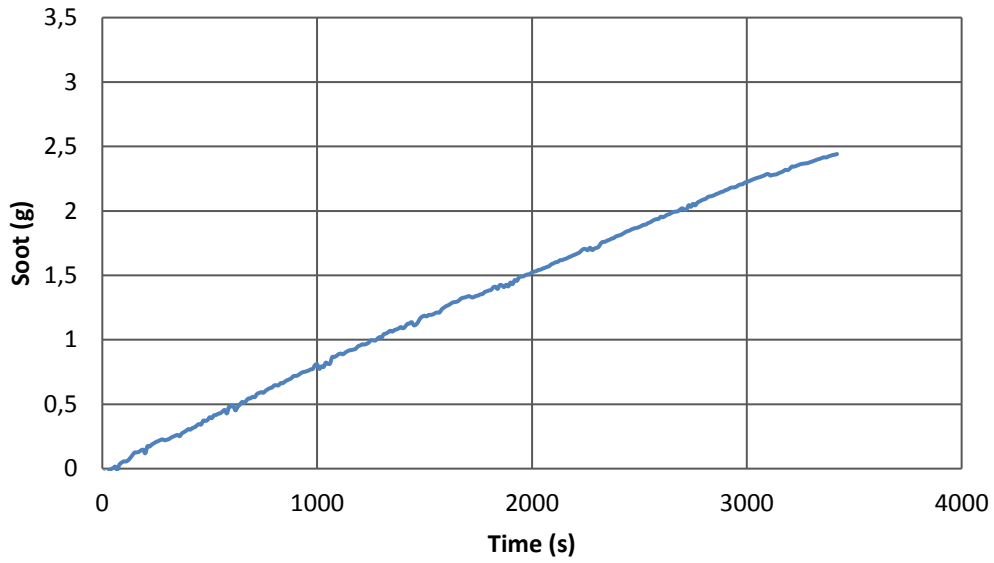

Figure 54:Soot as a function of time for the early SOI test 1 condition testing as obtained from the surface fitting model.

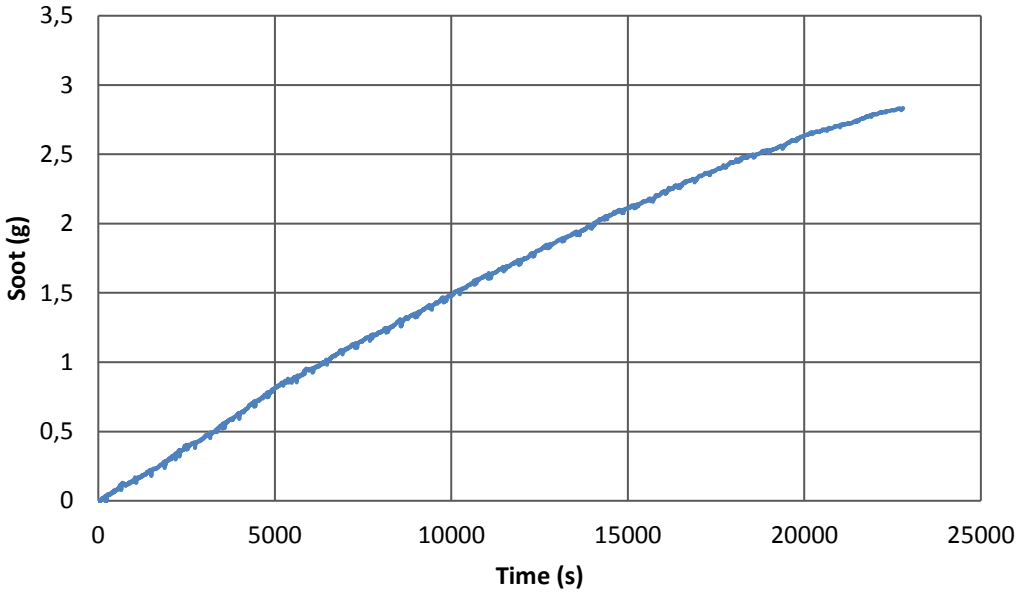

Figure 55:Soot as a function of time for the late SOI tenting conditions as obtained from the surface fitting model.

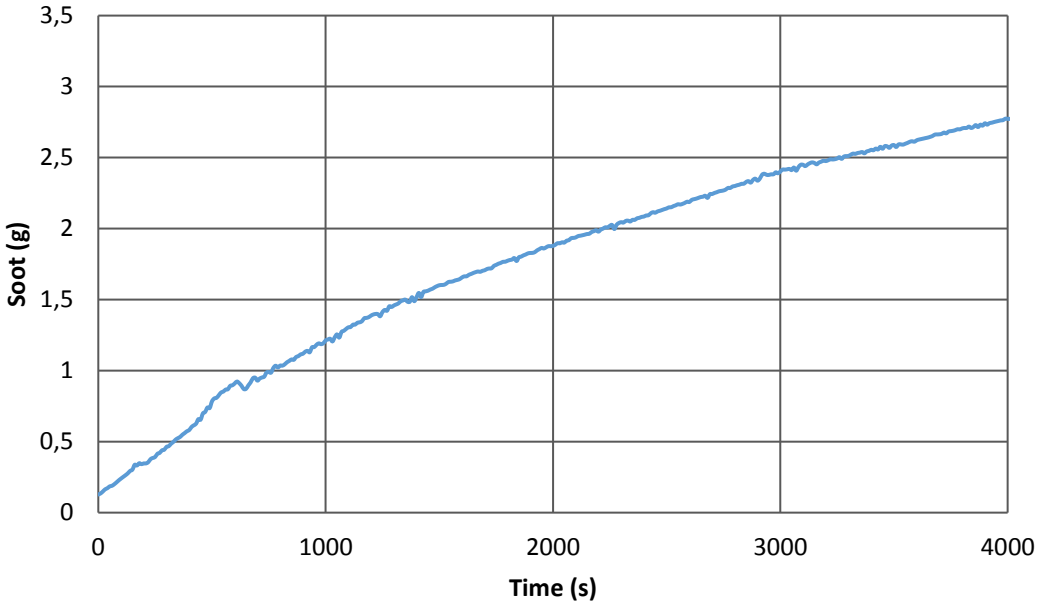

Figure 56:Soot as function of time for the early SOI test 2 conditions as obtained from the surface fitting model.

Table 13: Values of the soot weights, amount of soot predicted by the model and error.

Experiment	Weighed soot	Predicted soot	Error
Early SOI test 1	2.5 g	2.4 g	4 %
Late SOI	2.5 g	2.8 g	16 %

The trends in early SOI Test 1 is slightly different from early SOI Test 2 which has a more parabolic shape; this is because the latter test lasted more and the final amount of soot is higher and closer to the limits of the GPF filtration capacity.

In the case of late SOI the curve shape is still parabolic, but it is harder to see it because the process lasted a long time, and the curvature is less pronounced.

in Figure 57 the curves presenting soot as a function of the average forward gain for the early SOI and late SOI tests are shown. They are superimposed and the radio frequency sensor output is equal for the same amount of soot even if SOIs and T_e are different. Consequently, the model

is not dependent on the injection operating conditions and it is compensated for temperature variation.

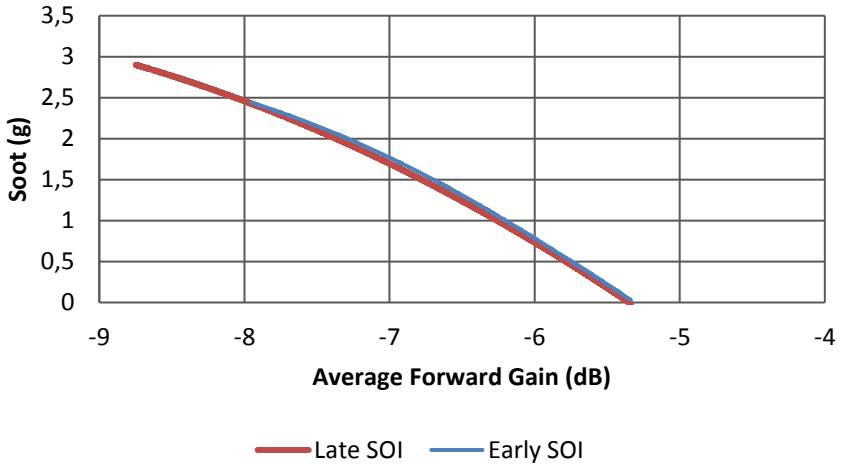

Figure 57:Soot as a function of average forward gain for late SOI and early SOI conditions.

Another result is shown in Figure 58, where the two soot accumulation trends obtained from the model for the two early SOI tests, are presented as function of the average forward gain given as output by the radio frequency sensor. It is possible to notice that the two curves are almost equal, even if the two tests were performed with a time difference of one month and the Radio Frequency sensor antennas were dismounted and mounted again in the GPF. From this comparison, it is acceptable to say that using the radio frequency sensor gives repeatable results.

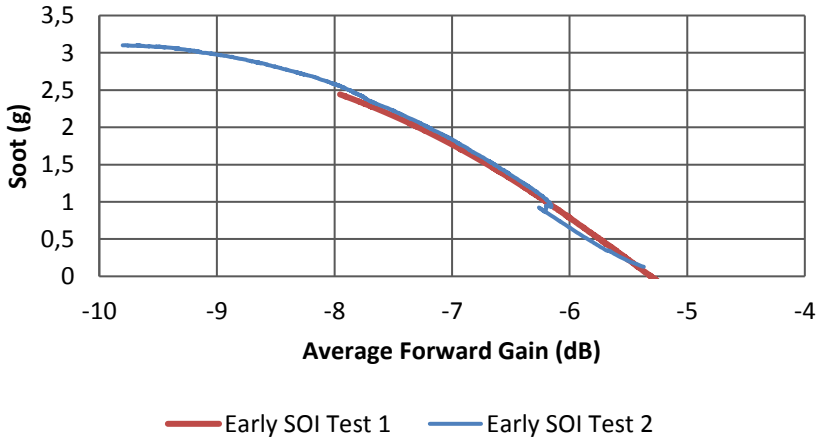

Figure 58: Soot values as function of average forward gain in the two cases of early SOI tests.

5.5 Results – Regeneration

The output obtained with the model in the early SOI, late SOI and low injection pressure regeneration cases are shown in Figure 59, Figure 60 and Figure 61. The amount of soot is presented as function of time. Then a graph showing the comparison between the three different soot oxidation trends is presented. In all graphs, it is possible to notice that as far as the temperature reaches ≈500 °C the soot starts to be oxidized.

Figure 59 presents the oxidation evolution in time for the early SOI produced soot. According to what discussed in the methodology section (Figure 32), this soot was expected to be less reactive than the other operating conditions; in fact, one hour was not enough to completely oxidize all soot accumulated in the GPF. At the end of the regeneration process there is some residual soot on the filter.

Figure 60 shows the results obtained for the late SOI produced soot. In this case soot is completely oxidized much before the end of the regeneration phase suggesting that the direct measurements of the radio frequency sensor may also be used as an indicator for the optimal duration of regeneration event.

In Figure 61 the soot oxidation process for the low injection pressure produced soot is reported. Again, from this graph it is possible to say that regeneration lasted more time than necessary to remove the soot.

In the three graphs the soot oxidation trend is slower at the beginning and when temperature stabilizes around 566°C for early SOI and late SOI tests and 580°C for the low injection pressure test the process is faster as found in literature [20].

The most interesting result is shown in Figure 62, where the normalized results of soot oxidation for the two different operating conditions (early and late SOI) are in the same graph together to be compared. For these two tests T_e during the oxidation process was 566 °C. Low injection pressure regeneration normalized result is not shown in the same graph because oxidation happened at higher T_e (580 °C). Temperature has been demonstrated to strongly affect the oxidation rate; with an increase of temperature (500 °C to 550 °C) the oxidation rate doubles. Then the three tests cannot be compared all together.

Analyzing Figure 62, the early SOI soot produced took the greatest time to be oxidized, whereas the results from late SOI and low injection pressure tests show that the oxidation rate is very similar, and faster compared to early SOI. It is finally possible to say, that based on this calibration different soot reactivity can be distinguished; in fact, the obtained output has slope characteristics that depend on the loading test conditions.

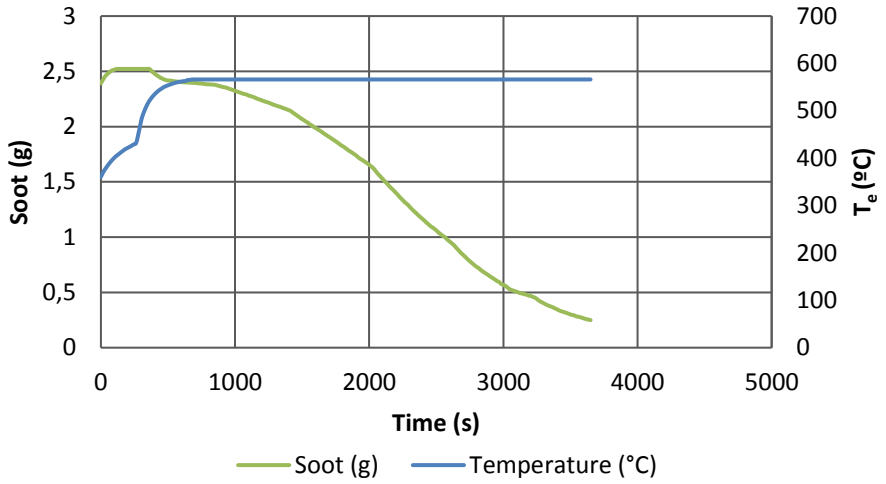

Figure 59: Soot oxidation trend obtained from the model in the case of early SOI produced soot and T_e trend as function of time during regeneration phase.

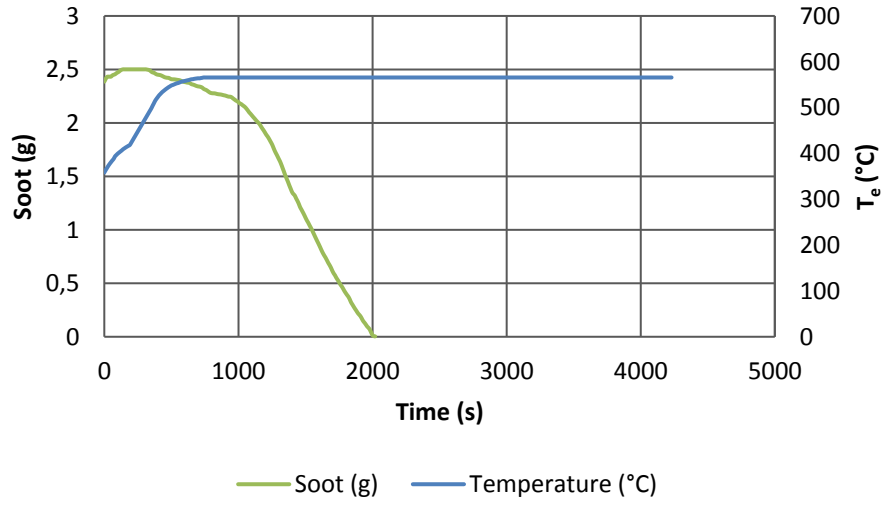

Figure 60: Soot oxidation trend obtained from the model in the case of late SOI produced soot and T_e trend as function of time during regeneration phase.

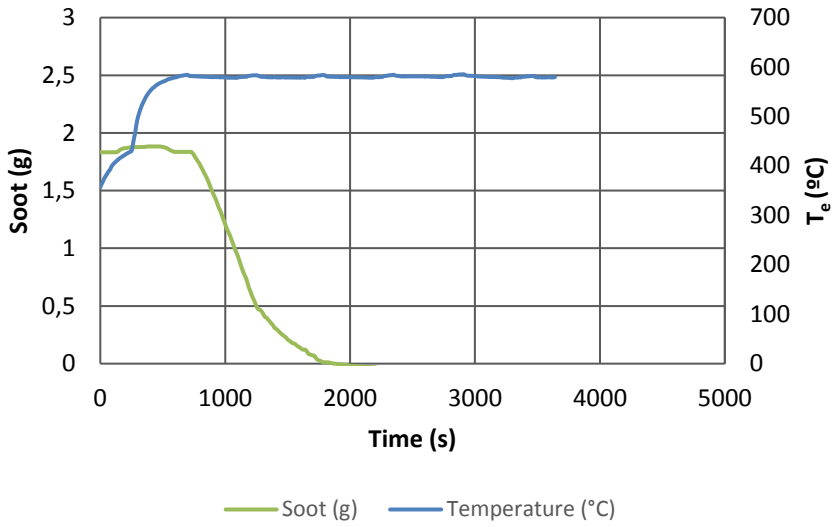

Figure 61: Soot oxidation trend obtained from the model in the case of low injection pressure produced soot and T_e trend as function of time during regeneration phase.

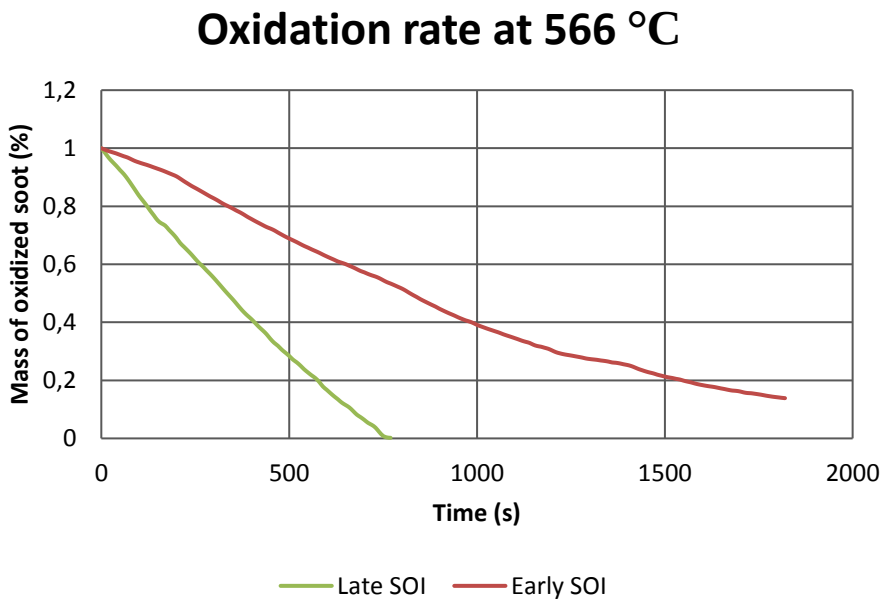

Figure 62: Comparison between normalized soot oxidation at 566 ºC for the three different operating conditions.

The last result from the model was obtained for the DFSO regeneration test. The regeneration started as usual and then fuel was cut off with consequent reduction of T_e, as discussed in the 4.4 paragraph. In Figure 63 the soot oxidation trend and the T_e trend as function of time are

shown, for the interval before the start of the fuel shut off. Soot starts to oxidize and about 0.18 grams are removed from the filter according to the simulation from the model. In Figure 64 the model outcome for the last part of regeneration event, after the happening of the DFSO, is presented. Both soot oxidation evolution and T_e at the inlet of the GPF are shown. In this case, soot oxidation seems to start later with respect to previous cases; this is probably due to the lower temperature of the GPF because of the DFSO.

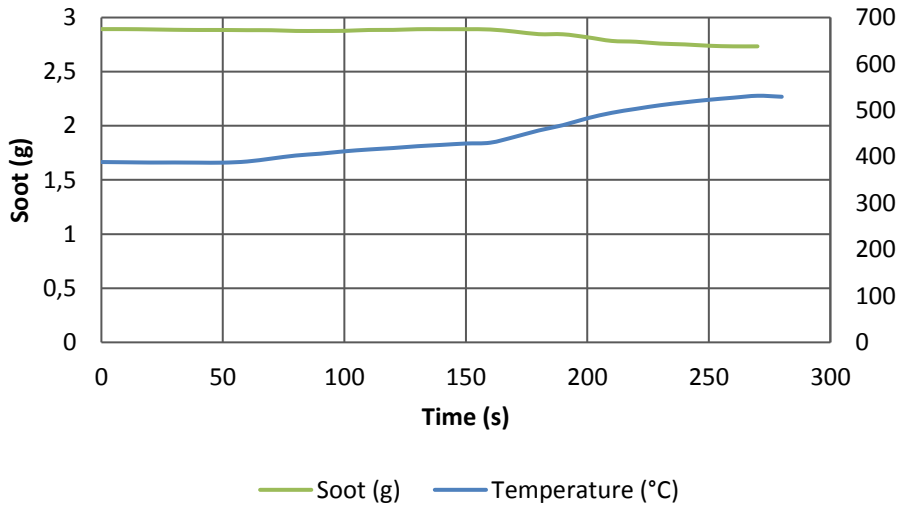

Figure 63: Soot oxidation as a function of time during regeneration of early SOI produced soot before the start of DFSO.

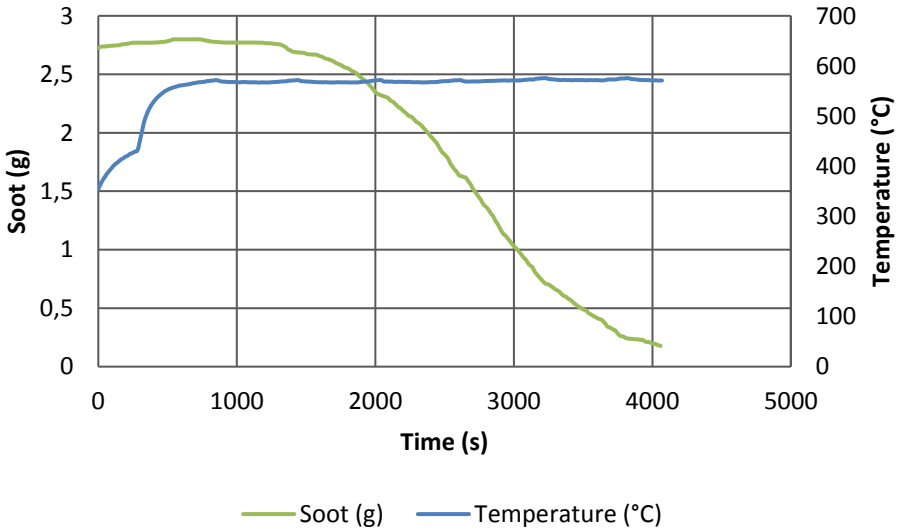

Figure 64: Soot oxidation as a function of time during regeneration of early SOI produced soot after the end of DFSO

6. CONCLUSIONS AND FUTURE WORK

In this chapter a summary of all the outcomes of this work will be presented. Moreover, some suggestions for improving the modeling and obtaining more detailed results will be given.

6.1 Conclusions

With this study a calibration of the Accusolve soot Radio Frequency sensor has been developed, to directly monitor soot accumulation in gasoline particulate filter in laboratory conditions environment. The Radio Frequency measurement system was installed on a 2.0 liters turbocharged gasoline direct injection engine and evaluated on three injection conditions, varying the start of injection and the injection pressure. Among the output provided by the Accusolve Radio Frequency sensor, the average forward gain was the parameter chosen for soot correlation. This value is influenced by the temperature of the filter, thus temperature compensation was performed by the model. Temperature, average forward gain and soot values from defined key points of three out of five tests were used for the creation of two maps (one for loading phase and one for regeneration phase) which were used for calibrating the model.

Analysis of the results from the model provide information on the amount of soot present in the filter during loading and regeneration phases and on the soot oxidation rate dependence on different injection conditions. Moreover, the bare results from the Radio Frequency sensor were compared to those obtained with the differential pressure sensor, which is the most used device for soot estimation and for triggering regeneration events.

The following outcomes have been obtained:

- It was found that the set RF sensor frequency range that worked for DPFs application is not working for GPFs; the appropriate frequency range for this application is from 2.135 GHz to 2.2 GHz;
- A model which simulates the soot accumulation during the loading phase was built; it correlates temperature, average forward gain and soot amount. In the model, temperature (first independent variable) contributes with first order and average forward gain (second independent variable) contributes with second order;

- The final value of soot predicted by the model during the loading phase show an error of 4% in the case of early SOI test 1 and 16% in the case of late SOI;
- For the regeneration event, a separate model was developed with different contribution of the two independent variables; temperature contributes with second degree and average forward gain with -1 degree;
- The soot oxidation rate predicted by the model can be considered realistic; in fact, soot starts to oxidize faster at the beginning, and then the process slows down because soot becomes harder to be oxidized;
- Finally, it was found that the oxidation rate is related to the injection conditions in which the soot was produced, because they determine the reactivity of the soot. Then, using the Radio Frequency sensor it is possible to identify the different type of soot;

6.2 Future work

The models developed for this work were defined for the uncoated filter; the influence of the catalyst should be studied more in details testing the coated filter, to understand how it affects the signal of the Radio Frequency sensor.

All tests for developing this study were performed at constant engine speed and torque; consequently, only a certain temperature range (350÷570 °C) was considered for the temperature compensation of the model; a suggestion would be to vary engine parameters to have a wider temperature operation range of the model. Moreover, weight procedure could be performed not only at the end of the experiment, but more times during it; a more accurate approximation of the soot estimation would be reached.

Temperature data for the creation of the model were obtained using a K thermocouple which measured the T_e at inlet and outlet of the GPF; these values were used as approximation of the filter temperature. It would be more appropriate to propose a model which uses these two temperatures to determine the filter temperature, by simulating the heat transfer between the exhaust gas and the monolith.

In total, five experiments were carried out to complete the model development, three for early SOI, one for late SOI and one for low injection pressure conditions; more experiments could confirm the repeatability of the Radio Frequency sensor measurements.

This study has been performed for Radio Frequency sensor application in laboratory environment; as last suggestion, it would be interesting to experiment the actual use of this typology of sensors for on-road application. The possibility of having a direct correlation with soot amount present in the filter (both GPFs and DPFs) could help for optimizing regeneration triggering and duration.

APPENDIX

Appendix A

GPF WEIGHING METHOD

One of the steps of the testing process, is the weighing of the gasoline particulate filter. After the filter is dismounted, this procedure is followed:

1. Scale is turned on and it is calibrated with a metal plate;
2. The GPF, which is at high temperature, is positioned on the scale and the weight is recorded;
3. The GPF is removed and the scale is zeroed;
4. The weighing and zero procedure is repeated three times;
5. Temperature is recorded with a thermocouple inserted near the brick face;
6. The GPF is cooled down in air for five minutes;
7. The procedure from point 3 to 5 is repeated, so that three measurements on the GPF at high temperature and three at low temperature are recorded.

Figure 65 shows the setting of GPF scale and thermocouple used for the weighing procedure.

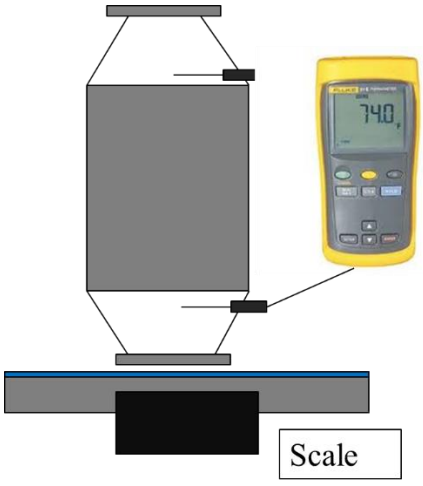

Figure 65: Schematic configuration of weighing apparatus.

When the filter is cooled down, the soot absorbs water and its weight increases; hence filter weight depends on temperature. For this reason, a temperature normalization is performed using soot data collected during the final test. During the final test, the uncoated filter was

measured three times; the soot values with the relative recorded temperatures are reported in Table 14.

Table 14: Uncoated GPF weight values with relative temperature recorded during the final test.

GPF	Condition	Weight 1 (g)	Weight 2 (g)	Weight 3 (g)	Average	Std Dev	Temperature
Uncoated	25 min early SOI	2203.8	2203.6	2203.7	2203.7	0.1	T=126 °C
Uncoated	25 min early SOI	2204.2	2204	2203.8	2204	0.2	T=68 °C
Uncoated	75 min early SOI	2205.1	2205	2205.1	2205.1	0.1	T=112 °C
Uncoated	75 min early SOI	2205.4	2205.4	2205.4	2205.4	0.0	T=62 °C
Uncoated	100 min early SOI	2205.7	2205.6	2205.4	2205.6	0.2	T=129°C
Uncoated	100 min early SOI	2205.9	2205.8	2205.8	2205.8	0.1	T=90 °C

GPF weights were plotted as function of temperature, to verify how temperature affects the weights for the different soot mass accumulated; it was found that there is no dependence on the amount of soot loaded.

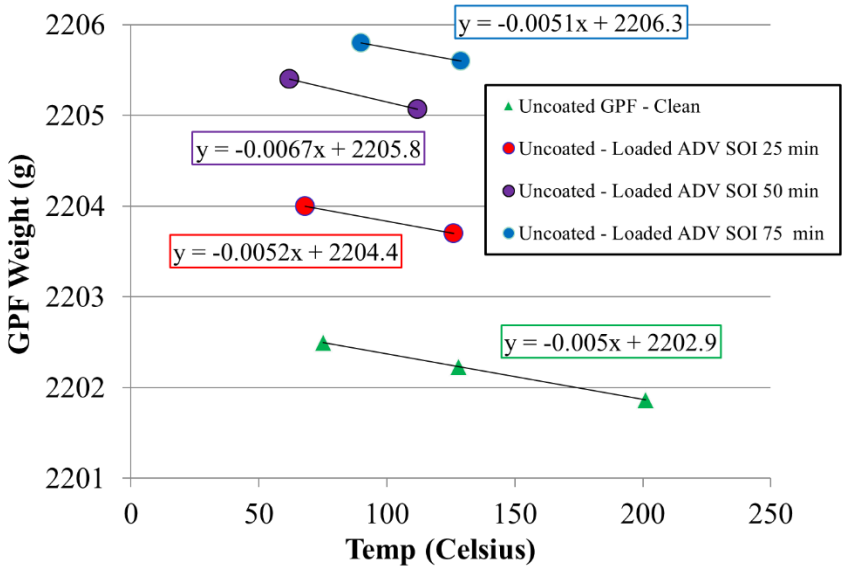

Figure 66: GPF weights as a function of temperature, collected during the final test for the uncoated GPF.

Then, a new dataset was created, considering slopes in the range 0.005, 0.006 and 0.007, temperature in the range 75÷200 °C and GPF weight 2200÷2201 grams. The plot obtained with this dataset is shown in Figure 67. The highest standard deviation for the GPF weights was found to be 0.125 at 75 °C.

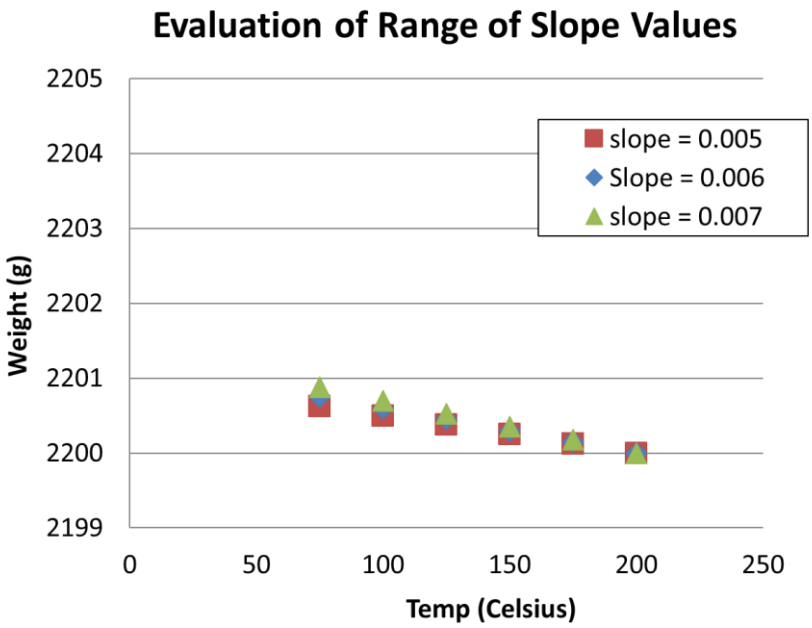

Figure 67: Plot of the dataset created to normalize GPF temperature.

To conclude, it was decided to normalize the GPF weights using a slope of 0.006 and a temperature of 150 °C. The normalized results are shown in Table 15.

Table 15: Final test weights for the uncoated GPF normalized with respect to temperature.

GPF	Condition	Weight (g)	Temperature (°C)
Uncoated	25 min early SOI	1.42	150
Uncoated	75 min early SOI	2.75	150
Uncoated	100 min early SOI	3.35	150

Appendix B

TABLES FOR LOADING AND REGENERATION MODEL CREATION

In this appendix, the two tables used for the generation of the loading and regeneration model are presented. Notice that for the regeneration model dataset, there are more data because it was necessary to compensate for temperature in the transient phase.

Table 16: Dataset used for the creation of the model for the loading phase.

Soot (gr)	Temperature (°C)	RF (dB)
0.00	352.47	-5.43
0.00	400.03	-5.54
0.00	504.14	-5.87
0.00	559.87	-5.31
1.42	350.81	-6.31
1.42	390.28	-6.67
1.90	350.81	-6.49
1.90	399.06	-6.72
1.90	506.31	-8.18
2.50	352.54	-7.84
2.50	401.90	-8.33
2.50	503.88	-10.82
2.75	351.26	-7.75
2.75	396.13	-8.42
3.35	403.83	-9.50

Table 17: Dataset used for the creation of the model for the regeneration phase.

Soot (gr)	Temperature (°C)	RF (dB)
0.00	411.24	-5.18
0.00	559.87	-5.31
0.00	579.37	-5.99
1.90	350.81	-6.49
1.90	357.18	-6.51
1.90	363.00	-6.55
1.90	368.01	-6.57
1.90	373.49	-6.59
1.90	378.41	-6.60
1.90	382.08	-6.63
1.90	386.36	-6.65
1.90	390.01	-6.66
1.90	393.37	-6.70
1.90	399.06	-6.72
1.90	405.22	-6.76
1.90	407.63	-6.78
1.90	409.89	-6.80
1.90	412.25	-6.81
1.90	414.29	-6.84
1.90	416.41	-6.85
1.90	417.89	-6.87
1.90	419.62	-6.90
1.90	421.01	-6.91
1.90	422.96	-6.93
1.90	424.63	-6.94
1.90	426.02	-6.93
1.90	427.30	-6.95
1.90	428.72	-6.97
1.90	430.10	-7.09
1.90	442.13	-7.22
1.90	456.05	-7.37
1.90	468.05	-7.60
1.90	485.24	-7.79
1.90	496.86	-7.99
1.90	506.31	-8.18
2.50	352.54	-7.84
2.50	358.38	-7.89
2.50	363.46	-7.93
2.50	368.33	-7.98

Soot (gr)	Temperature (°C)	RF (dB)
2.50	373.01	-8.02
2.50	377.21	-8.07
2.50	381.08	-8.11
2.50	384.77	-8.16
2.50	388.29	-8.19
2.50	393.60	-8.24
2.50	396.66	-8.27
2.50	399.58	-8.30
2.50	401.90	-8.33
2.50	404.27	-8.37
2.50	406.52	-8.41
2.50	409.18	-8.44
2.50	411.11	-8.47
2.50	413.18	-8.50
2.50	414.95	-8.51
2.50	416.71	-8.55
2.50	418.35	-8.57
2.50	419.50	-8.62
2.50	420.77	-8.65
2.50	422.60	-8.66
2.50	424.11	-8.71
2.50	425.57	-8.72
2.50	426.65	-8.74
2.50	427.79	-8.77
2.50	429.09	-8.81
2.50	429.99	-8.87
2.50	431.36	-9.03
2.50	441.08	-9.27
2.50	454.31	-9.58
2.50	466.39	-9.86
2.50	480.15	-10.11
2.50	489.72	-10.36
2.50	496.94	-10.59
2.50	503.88	-10.82
2.75	351.26	-7.75
2.75	396.13	-8.42
3.35	403.83	-9.50

REFERENCES

[1] O. Bulent and M. B. Çelik, "Gasoline Direct Injection, Fuel Injection InTech, Available from: http://www.intechopen.com/books/fuelinjection/gasoline-direct-injection.," Daniela Siano (Ed.), 2010.

[2] F. Zhao, M. C. Lai and D. Harrington, "Automotive spark-ignited direct-injection gasoline engines," in *Progress in Energy and Combustion Science*, 1999, pp. 437-562.

[3] J. Richter, R. Klingmann, S. Spiess and K. Wong, "Application of Catalyzed Gasoline Particulate Filters to GDI Vehicles," SAE Int. J. Engines 2012-01-1244, 2012.

[4] I. Khalek, "Particle Emissions from Direct Injection Gasoline Engines," *Technology Today,* 2011.

[5] Y. Ito, T. Shimoda, T. Aoki, K. Yuuki and e. al., "Next Generation of Ceramic Wall Flow Gasoline Particulate Filter with Integrated Three Way Catalyst," SAE Technical Paper 2015-01-1073, 2015.

[6] CARB, "Final Regulation Order, LEV III Amendments," California Code of Regulations, 2012.

[7] EU, "Commission Regulation (EU) 2016/427," *Official Journal of the European Union,* vol. 82, pp. 1-98, 2016.

[8] A. Sappok, P. Ragaller, L. Bromberg and V. Prikhodko, *Real-Time Engine and Aftertreatment System Control Using Fast Response Particulate Filter Sensors,* SAE Technical Paper 2016-01-0918, 2016.

[9] T. Kume, Y. Iwamoto, K. Iida, M. Murakami, K. Akishino and H. Ando, *Combustion control technologies for direct injection SI engine,* SAE Technical Paper 960600, 1996.

[10] G. Karl, R. Kemmler and M. Bargende, *Analysis of a direct injected gasoline engine,* SAE Technical Paper No. 970624, 1997.

[11] C. L. Myung and S. Park, "Exhaust nanoparticle emissions from internal combustion engines: A review.," *Int. J. Automotive Technology,* vol. 1, pp. 9-22, 2012.

[12] M. Braisher, R. Stone and P. Price, *Particle number emissions from a range of European vehicles,* SAE Paper No. 01-0786, 2010.

[13] D. B. Kittleson, "Engines and nanoparticles: a review.," *J Aerosol Sci,* vol. 29, pp. 575-88,

1998.

[14] C. A. Amann and D. C. Siegla, "Diesel Particulates-What They Are and Why.," *Aerosol Sci. Technol.,* vol. 1, pp. 73-101, 1982.

[15] H. Seong, S. Choi and K. Lee, "Examination of nanoparticles from gasoline direct-injection (GDI) engine using transmission electron microscopy (TEM)," *Int. J. Automotive Technolog,* vol. 2, no. 15, pp. 175-181, 2014.

[16] S. Choi and H. Seong, "Lube oil-dependent ash chemistry on soot oxidation reactivity in a gasoline direct-injection engine," *Combustion and Flame,* vol. 174, pp. 68-76, 2016.

[17] R. Wal and A. Tomasek, "Soot Oxidation Dependence Upon Initial Nanostructure," *Combustion Flame,* pp. 1-9, 2003.

[18] P. H.B. and C. C.F., in *The Chemistry and Physics of Carbon*, New York, Marcel Dekker, 1965, p. 265.

[19] A. Kandas, I. Senel, Y. Levendis and A. Sarofim, "Soot Surface Area Evolution During Air Oxidation as Evaluated by Small Angle X-Ray Scattering and CO2 Adsorption," in *Carbon*, 2005, pp. 241-251.

[20] H. Seong, K. Lee and S. Choi, "Effects of Engine Operating Parameters on Morphology from a Gasoline Direct Injection (GDI) engine soot: Catalytic effects of ash and modified kinetic correlation," *Combustion and Flame,* vol. 162, pp. 2371-2389, 2015.

[21] T. W. Chan, E. Meloch, D. Rosenblat, J. Kubsh, B. R. and G. Rideout, "Reducing Particulate Emissions for Future Gasoline Direct Injection Vehicles with a Gasoline Particulate Filter," in *16th ETH-Conference on Combustion Generated Nanoparticles*, Zurich, Switzerland, 2012.

[22] T. W. Chan, M. Saffaripour, F. Liu, J. Hendren, K. A. Thomson, J. Kubsh, R. Brezny and G. Rideout, "Characterization of Real-Time Particle Emissions from a Gasoline Direct Injection Vehicle Equipped with a Catalyzed Gasoline Particulate Filter During Filter Regeneration," *Emission Control Sci. Technol.,* pp. 75-88, 2016.

[23] M. Masoudi and A. G. Sappok, "DieselNet Soot (PM) Sensors," 8 April 2017. [Online]. Available: https://www.dieselnet.com/tech/sensors_soot.php. [Accessed 2017].

[24] W. A. Majewski, "Dieselnet - Diesel Particulate Filters," 18 January 2013. [Online]. Available: https://www.dieselnet.com/tech/dpf.php. [Accessed 2017].

[25] D. Waters, D. Thier, Y. Ito, M. Yamashita, C. Vogt, K. Kato, T. Shimoda, T. Aoki and M. Makino, *Performance of advanced Gasoline Particulate Filter Material for Real Driving*

Conditions.

[26] C. Saito, T. Nakatani, Y. Miyairi, K. Yuuki, M. Makino, H. Kurachi, W. Heuss, T. Kuki, Y. Furuta, P. Kattouah and C. Vogt, *New particulate filter concept to reduce particle number emissions,* SAE Tech. Paper, 2011-01-0814, 2011.

[27] M. Görgen, S. Sterlepper, S. Herrmann, M. Hendrikx, M. Nijs and J. Scharf, *Gasoline Particulate Filters Market and Technology Trends and their Impact on Calibration,* FEV Technical Paper, 2017.

[28] Robert Bosch GmbH internal, ""“Product information – Differential Pressure Sensor DS-D2"," 2002.

[29] W. Majewski, "DieselNet Diesel FIlter Systems," 11 November 2015. [Online]. Available: https://www.dieselnet.com/tech/dpf_sys.php. [Accessed 2017].

[30] H. Nanjundaswamy, V. Nagaraju, Y. Wu and E. Koehler, *Advanced RF Particulate Filter Sensing and Controls for Efficient Aftertreatment Management and Reduced Fuel Consumption,* SAE Technical Paper 2015-01-0996, 2015.

[31] Amphenol, *Accusolve Advanced Diesel Particulate Filter Soot Sensor Performance Evaluation Guide,* 2014.

[32] P. Y. Yu and C. M., in *Fundamentals of Semiconductors: Physics and Materials Properties*, Berlin, Springer, 2001, p. 261.

[33] A. Sappok, L. Bromberg, J. Parks and V. Prikhodko, *Loading and Regeneration Analysis of a Diesel Particulate Filter with a Radio Frequency-Based Sensor,* SAE Technical Paper 2010-01-2126, 2010.

[34] A. Sappok and L. Bromberg, "Development of Radio Fequency sensing for in-situ diesel particulate filter state monitoring and aftertreatment system control," in *ASME 2013 Internal Combustion Engine Division Fall Technical Conference*, 2013.

[35] A. Sappok and L. Bromberg, "Radio Frequency Diesel Particulate Filter Soot and Ash Level Sensors: Enabling Adaptive Controls for Heavy-Duty Diesel Applications," *SAE Int. J. Commer. Veh. ,* vol. 2, no. 7, 2014.

[36] M. Feulner, F. Seufert, A. Muller, G. Hagen and R. Moos, "Influencing Paramenters on the Microwave-Based Soot Load Determination of Diesel Particulate Filter," *Springer US,* vol. 60, no. 3-5, pp. 374-380, 2016.

[37] J. Hansson and V. Ingeström, *A Method for Estimating Soot Load in a DPF using an RF-based*

sensor, Linköpings universitet, Sweden, 2012.

[38] M. Feulner, A. Müller, G. Hagen, D. Brüggemann and R. Moos, "Microwave-Based Diesel Particulate Filter Monitoring – Soot Load Determination and Influencing Parameters," in *AMA Conferences 2013 - SENSOR 2013*, 2013.

[39] C. Cubito, *Sviluppo di metodologie per la previsione di emissioni inquinanti e consumo di combustibile da motori diesel automobilistici,* Politecnico di Torino Master Thesis, 2013.

VITA AUCTORIS

NAME:	Angela Fiano
PLACE OF BIRTH:	Caserta, Italy
YEAR OF BIRTH:	1993
EDUCATION:	Liceo scientifico L. Garofano, Capua, Italy, 2012
	Politecnico di Torino, Torino, Italy, 2015
	University of Windsor, M.Sc., Windsor, ON, 2017
	Politecnico di Torino, Torino, Italy, 2017